

An updated survey of globular clusters in M 31. III. A spectroscopic metallicity scale for the Revised Bologna Catalog^{*}.

S. Galleti¹, M. Bellazzini¹, A. Buzzoni¹, L. Federici¹, and F. Fusi Pecci¹

INAF - Osservatorio Astronomico di Bologna, Via Ranzani 1, 40127 Bologna, Italy
e-mail: silvia.galleti@oabo.inaf.it, michele.bellazzini@oabo.inaf.it, luciana.federici@oabo.inaf.it,
alberto.buzzoni@oabo.inaf.it, flavio.fusipecci@oabo.inaf.it

Received 27 May 2009 / Accepted 17 September 2009

ABSTRACT

Aims. We present a new homogeneous set of metallicity estimates based on Lick indices for the old globular clusters of the M31 galaxy. The final aim is to add homogeneous spectroscopic metallicities to as many entries as possible of the Revised Bologna Catalog of M31 clusters^{**}, by reporting Lick indices measurements from any source (literature, new observations, etc.) into the same scale.

Methods. New empirical relations of $[\text{Fe}/\text{H}]$ as a function of $[\text{MgFe}]$ and Mg2 indices, as defined by Trager et al. (1998), are based on well studied Galactic Globular Clusters, complemented with theoretical model predictions for $-0.2 \leq [\text{Fe}/\text{H}] \leq +0.5$. Lick indices for M31 clusters from various literature sources (225 clusters) and from new observations by our team (71 clusters) have been transformed into the Trager et al. (1998) system, yielding new metallicity estimates for 245 globular clusters of M31.

Results. Our values are in good agreement with recent estimates based on detailed spectral fitting and with those obtained from Color Magnitude Diagrams of clusters imaged with the Hubble Space Telescope. The typical uncertainty on individual estimates is $\approx \pm 0.25$ dex, as resulted from the comparison with metallicities derived from Color Magnitude Diagrams of individual clusters.

Conclusions. The metallicity distribution of M31 globular cluster is briefly discussed and compared with that of the Milky Way. Simple parametric statistical tests suggest that the distribution is likely not unimodal. The strong correlation between metallicity and kinematics found in previous studies is confirmed. The most metal-rich GCs tend to be packed at the center of the system and to cluster tightly around the galactic rotation curve defined by the HI disk, while the velocity dispersion about the curve increases with decreasing metallicity. However, also the clusters with $[\text{Fe}/\text{H}] < -1.0$ display a clear rotation pattern, at odds with their Milky Way counterparts.

Key words. Galaxies: individual: M 31 – Galaxies:star clusters – catalogs — Galaxies: Local Group

1. Introduction

The concept of Simple Stellar Population (SSP) has proven to be a very fruitful tool for the study of virtually any kind of stellar system (Renzini & Buzzoni 1986; Renzini & Fusi Pecci 1988, hereafter RFP88). A SSP is completely characterized by only four “parameters”: (a) mass, (b) chemical composition, (c) age, and (d) mass function, that determines the mass to light ratio (M/L) of the SSP once fixed the age and the chemical composition (see RFP88, for further possibly relevant variables that are not considered at zero-approximation). As a further simplification, the chemical composition is typically represented with two main parameters, i.e. the Helium abundance (Y) and the total abundance of elements heavier than He, usually parametrized by the iron abundance $[\text{Fe}/\text{H}]$ (see, for instance Zinn & West (1984) (ZW84), Tantaló & Chiosi (2004b,a) and references therein). Even if the abundance of the so called α -elements has been

subject of an increasing interest in the last two decades (McWilliam 1997; Thomas et al. 2004; Tantaló & Chiosi 2004a; Gratton, Sneden & Carretta 2004) $[\text{Fe}/\text{H}]$ remains the main parameter to rank stars and/or stellar populations according to their abundance of heavy elements.

In the study of globular clusters (GC), which are the best approximation of a SSP in nature, the metallicity is a key parameter that is also needed to infer ages and age differences (see, for example RFP88 and Carretta & Gratton 1997, and references therein). The knowledge of the metallicity of a large sample of globular clusters in a given galaxy allows one to search for metallicity gradients, and the presence of distinct sub-populations of GCs (as in the Milky Way (MW) Zinn (1985), and in many external galaxies Brodie & Strader (2006)), and, in general, to obtain crucial information on the early phases of the formation and chemical enrichment of the parent galaxy.

While modern instrumentation has allowed the determination of the detailed abundance of several elements in single stars belonging to GCs of the MW (see Sneden 2005; Gratton, Sneden & Carretta 2004; Carretta et al. 2008), the metallicities of extragalactic GCs must be obtained from their integrated colors and/or spectra, by comparison with Galactic templates and/or theoretical models (Brodie & Strader 2006). Several broad-band integrated colors are fairly sensitive to metallicity and relatively easy to measure for clusters out to very large distances. However, they suffer from the well-

Send offprint requests to: S. Galleti

^{*} Based on observations made at La Palma, at the Spanish Observatorio del Roque de los Muchachos of the IAC, with the William Herschel Telescope of the Isaac Newton Group and with the Italian Telescopio Nazionale Galileo (TNG) operated by the Fundación Galileo Galilei of INAF. Also based on observations made with the G.B. Cassini Telescope at Loiano (Italy), operated by the Osservatorio Astronomico di Bologna (INAF).

^{**} RBC Version 4 available at: www.bo.astro.it/M31

known age-metallicity degeneracy (RFP88) and they may be badly affected by the reddening due to extinction by interstellar dust. While the foreground extinction associated with the dust layers residing in our own Galaxy may be somehow constrained by observations and modeled (Schlegel et al. 1998), the extinction intrinsic to external galaxies is largely unknown. On the other hand, spectral indices based on the strength of an absorption feature with respect to the surrounding continuum also suffer from the age-metallicity degeneracy (to different degrees, see Worthey 1994) but they are essentially unaffected by extinction (MacArthur 2005), a very desirable characteristic. The most widely used spectral indices were originally defined by Burstein et al. (1984) and Faber et al. (1985) at the Lick Observatory. These authors defined a set of indices that measure the strength of the most pronounced absorption features that are seen in the integrated low-resolution spectra of stellar systems at optical wavelengths. The use of Lick indices became widespread because they are easy to measure; as a consequence, they were also included as standard predictions in all theoretical models of SSP (see, for example, Buzzoni et al. (1992, 1994); Worthey (1994); Bruzual & Charlot (2003) hereafter BC03, Tantaló & Chiosi (2004b); Thomas et al. (2003), hereafter TMB).

The M31 galaxy is an ideal target for studying GCs. It is nearby and it has a large cluster population (~ 3 times larger than the MW). The globular cluster system of M31 has been intensively studied in the past and several authors have used Lick indices to constrain the age and the metallicity of clusters in the Andromeda Galaxy.

Integrated-light spectroscopy of M31 GCs was pioneered by van den Bergh (1969) who found that the GC system of this galaxy extends to higher metallicities with respect to the MW. In an important contribution, Burstein et al. (1984) comprehensively discussed other interesting differences between GCs in M31 and in the MW. In particular they showed that M31 clusters have significantly stronger H β and CN absorption indices at a given metallicity. In a series of papers Brodie & Huchra (1990, 1991) and Huchra et al. (1991) studied the metallicity distribution of M31 GCs using an extensive sample of integrated spectra and line indices. They found that the properties of the M31 GC system are broadly similar to the MW one, but they confirmed the presence of a high-metallicity tail having no counterpart in our Galaxy. They found that the mean metallicity [Fe/H] was -1.2 , and they identified a weak metallicity gradient as a function of projected radius. From the distribution of integrated colors Barmby et al. (2000) found evidences that the M31 GC system may have a bimodal metallicity distribution (like the Milky Way, Zinn 1985), with peaks at [Fe/H] ~ -1.4 and [Fe/H] ~ -0.6 . Moreover, they found that the $(V-K)_0$ color distribution was best modeled assuming three modes in the metallicity distribution, instead of one or two. Finally, they found a small radial metallicity gradient and no correlation between cluster luminosity and metallicity in M31 GCs. Perrett et al. (2002) produced a total sample of about 200 spectroscopic metallicities of M31 GCs, calibrating Lick indices measured in their own system versus the metallicity of M31 clusters in common with Huchra et al. (1991) (hence they used a set of *secondary* calibrators). They confirmed the bimodality in the metallicity distribution and reported that the metal-rich clusters have a higher rotation amplitude with respect to metal-poor ones, while both groups are known to rotate faster than their Galactic counterparts. Moreover, they found evidence for a radial metallicity gradient in the metal-poor population of M31 out to $\sim 60'$ from the galaxy center.

Metallicity (and age) estimates for various samples of M31 clusters obtained by fitting spectra with theoretical SSP models have been recently presented by Beasley et al. (2005) and Puzia et al. (2005). Beasley et al. (2005) studied a sample of 23 M31 GCs with very high Signal to Noise (S/N) spectra, seventeen of which were found to be old and to span a large range of metallicity, while the remaining six were classified as intermediate age clusters. Puzia et al. (2005) presented the metallicity of 70 globular clusters (including those studied by Beasley et al. (2005)) finding a bimodal distribution with peaks at [Z/H] $\sim -1.66 (\pm 0.05)$ and [Z/H] $\sim -0.45 (\pm 0.04)$ dex with dispersions 0.23 and 0.29 dex, respectively¹.

More recently, Lee et al. (2008) merged the metallicities from Barmby et al. (2000) and Perrett et al. (2002) with their own estimates from the line indices measured from WIYN/Hydra spectra. They found that a bimodal and trimodal distribution are statistically preferable to a unimodal metallicity distribution at a confidence level of 99.8%. Fan et al. (2008) assembled metallicities from the literature and with estimates derived from integrated colors to obtain a global metallicity distribution of M31 GCs. They found a bimodal distributions with peaks at [Fe/H] ~ -1.7 and ~ -0.7 dex with mean [Fe/H] $= -1.21$ dex, but showed that three-group fits are also statistically acceptable. They found a metallicity gradient as a function of projected radius for the metal-poor GCs, but no gradient for the metal-rich GCs.

The brief summary of modern studies above underlines the great degree of heterogeneity of the available material. The various sets of estimates are obtained from observables that are different in nature (integrated spectral indices or colors) and are based on different calibrations (empirical, semi-empirical or theoretical; using primary or secondary calibrators). Even the actual definition of the same Lick indices varies from author to author; thus, in general, the presented calibrations are valid only for a given observational set-up and definition. In these circumstances it is clear that joining together different sets of metallicity estimates may be quite dangerous as it may lead to a poor degree of self-consistency in the final merged set.

We have assembled and we continuously maintain and update a database of parameters of confirmed and candidate clusters² in M31, the Revised Bologna Catalog of M31 globular clusters (RBC, Galleti et al. 2004, 2006a; Galleti et al. 2007). As we want to add a reliable metallicity estimate to the confirmed clusters in the RBC, we need to devise the operational protocol to transform the actual measures provided in the literature (as, for example, already available and future sets of Lick indices for M31 clusters) into a unique homogeneous metallicity scale. In this paper, we describe the construction of this new homogeneous metallicity scale for M31 GCs based on Lick line indices. Having set and tested the new scale, we present new metallicity estimates for 245 M31 GCs.

The plan of the paper is as follows. In Section 2, we describe the rationale and the procedure for the construction of the new metallicity scale. In Section 3, we report on the sample of M31 GC spectra that we have obtained and reduced, and from which we have estimated Lick indices. We also describe how we have collected Lick indices for M31 GCs from the literature and

¹ [Z/H] is defined as [Fe/H] + 0.94[α /Fe] taken from Thomas et al. (2003, see also Trager et al. 2000).

² We also keep lists of targets previously suggested as candidate M31 globular clusters and later found to be objects of different nature, like distant galaxies, foreground stars, regions HII etc., see Galleti et al. (2004, 2006a; Galleti et al. (2007).

how we have reported all of them to the same homogeneous system. Finally, we derive the new values of the metallicities and, in Section 4, compare our scale with previous metallicity estimates. In Section 5, we present and discuss the metallicity distribution of the M31 GC system and on the correlations between metallicity and kinematics.

2. An empirical metallicity scale

The construction of a metallicity scale must be driven by a list of basic requirements and a number of methodological/technical choices to achieve them, as well as some trade-off between different possibilities. In particular, we identified the following ranked list of desiderata.

1. The scale must be consistent with at least one of the main metallicity scales currently used for the Galactic GCs, like Zinn & West (1984, ZW84) or Carretta & Gratton (1997).
2. The scale must be calibrated on empirical templates. The agreement with theoretical predictions is clearly desirable but it is not a *must*, as theoretical models have problems and uncertainties on their own (Tantalo & Chiosi 2004a,b), while the chemical abundances of many Galactic GCs are known in great detail (Carretta et al. 2008).
3. The observables that are used to settle the scale must be as sensitive to the abundance of heavy elements as possible but also operationally well defined, and easy to measure out to large distances with currently available instrumentation.

Several authors have studied and discussed in detail the sensitivity of the various Lick indices to the abundance of various elements and to other parameters (see González 1993; Worthey 1994; Worthey et al. 1994; Worthey & Ottaviani 1997; Buzzoni et al. 1992; Buzzoni 1995b; Trager et al. 1998; Thomas et al. 2004, 2003; Tantalo & Chiosi 2004a,b, and references therein). Even if several indices are fairly sensitive to metallicity, they are not necessarily suitable to serve as the basis of a general purpose metallicity scale. As an extreme example, the $H\beta$ index is very sensitive to metallicity but it is also very sensitive to age, hence it would be a misleading metallicity indicator, in general. Fe4648, Fe5015, Fe5709, and Fe5782 have been indicated as very good metallicity indicators, but none of these absorption features seems ideal for reliable metallicity determinations. Fe4648 was found to be sensitive to C, O, Mg, and Si, hence it does not seem to trace any iron peak element. Fe5015 is mostly sensitive to iron, but it can be affected by $[OIII]$ emission. Fe5709 and Fe5782 are weak features which require very high S/N spectra to be reliably measured. There is general consensus that the most reliable (and easy to measure) iron-sensitive Lick indices are Fe5270 and Fe5335, as both measure predominantly strong iron lines. However all these features are relatively weak in most old SSP spectra with respect to the Mg features that are parametrized by the Mg2 and Mgb indices, both of which are shown to correlate very well with $[Fe/H]$ (Worthey (1994, 1996)).

As it became clear that old stellar populations (like GCs and classical elliptical galaxies) are characterized by an enhancement of α elements (N, O, Mg, Ca, Na, Ne, S, Si, Ti), or, better, by an iron deficiency with respect to the abundance pattern of the Sun, the impact of $[\alpha/Fe]$ on Lick indices has been the subject of detailed study (see Trager et al. 2000; Tantalo & Chiosi 2004a; Thomas et al. 2004, and references therein). To reduce the influence of $[\alpha/Fe]$ variations on age and metallicity determinations, González (1993) introduced the $[MgFe]$ index,

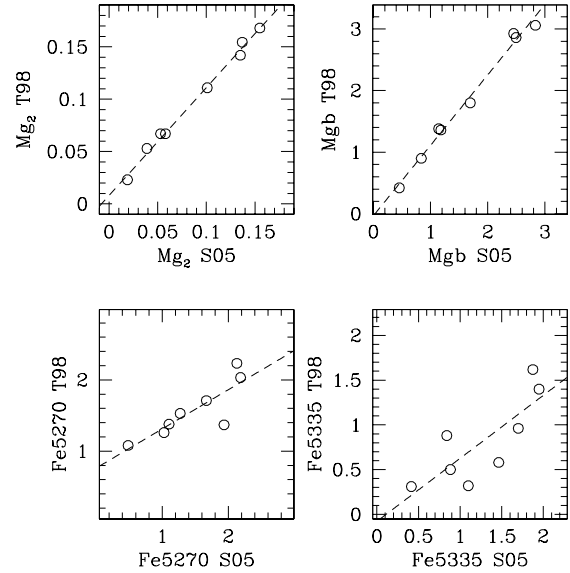


Fig. 1. Comparison of passband measurements from S05 spectra and original Lick data for 8 Galactic Globular Clusters. The dashed is a least-square fit to the open circles.

$[MgFe] = \sqrt{Mgb \cdot <Fe>}$ with $<Fe> = (Fe5270 + Fe5335)/2$, that appears to be very sensitive to the total metallicity while minimizing the dependency on $[\alpha/Fe]$ (see Thomas et al. 2004, 2003, for discussion).

After many tests using several indices we decided to base our scale on four indices: three of them (Mgb, Fe5270, and Fe5335) are combined into $[MgFe]$, the other is Mg2 (see Appendix B). Mg2 has become a standard "metallicity" indicator for the integrated spectra (see i.e. Buzzoni et al. (1992)). We found that $[MgFe]$ and Mg2 provide the most consistent and strong correlations with $[Fe/H]$ in the ZW84 scale, once the Trager et al. (1998, hereafter T98) definitions of the Lick indices are adopted. Therefore, to obtain a metallicity estimate in a reliable and homogeneous scale, the indices must be measured according to the T98 definitions and transformed into the T98 reference frame using a set of stars/stellar systems in common with T98 as standard calibrators (see Sect. 3, below). Operationally, when the spectrum of a given cluster has a sufficient signal-to-noise and wavelength coverage to allow a reliable measure of all the involved indices, including Fe5270 and Fe5335, the estimates of $[Fe/H]$ can be obtained from $[MgFe]$. A valid metallicity estimate can be obtained even if reliable measures of Fe5270 and Fe5335 are lacking; the use of both the assumed indicators is clearly preferable, but Mg2 alone is sufficient.

2.1. The calibrators

To fulfill simultaneously the requirements # 1 and # 2 above, we decided to adopt Galactic Globular clusters with metallicities in the ZW84 scale as fundamental calibrators. All the metallicity values for MW GCs adopted here are taken from ZW84 and Armandroff & Zinn (1988). It is clear that the choice of the calibrators implies that the scale is valid only for old populations having a similar degree of enhancement in the abundance of α -elements with respect to the Sun (see Pritzl et al. (2005)). We will use theoretical SSP models to explore the effective range of

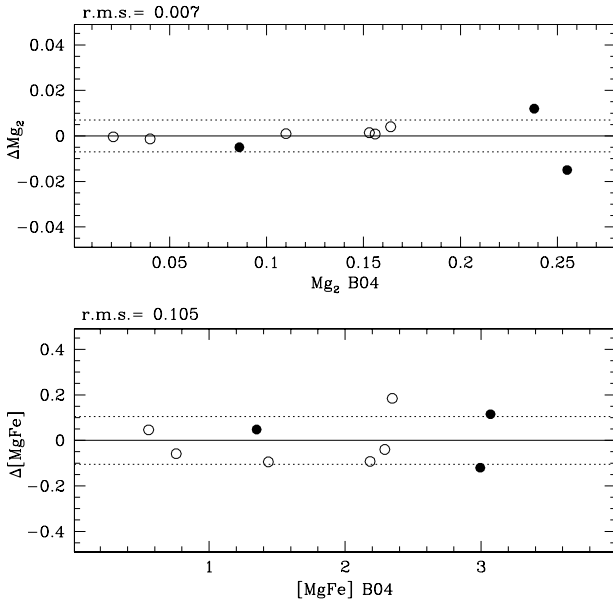


Fig. 2. Comparison of the metallicity line indices adopted (open circles are T98, filled circles are S05 data) with the B04 values transformed to T98 system. The rms of the distributions are also reported.

Table 1. Linear fit coefficients for transformations of the Schiavon data to the Lick system

Index	a	b	r.m.s.
Mg2	0.008	1.029	0.004
Mgb	-0.034	1.145	0.098
Fe5270	0.761	0.551	0.199
Fe5335	-0.079	0.704	0.275

Table 2. Linear fit coefficients for transformations of the Beasley data to the Lick system

Index	a	b	r.m.s.
Mg2	-0.008	1.002	0.006
Mgb	-0.051	1.076	0.187
Fe5270	0.377	0.757	0.217
Fe5335	-0.009	0.872	0.205

ages and chemical compositions in which our calibration can be considered valid.

We searched in the literature for assemble the largest possible sample of Galactic GCs with well known metallicity and having well measured Lick indices from high S/N spectra in the T98 system or that can be easily transformed into this system. First of all we took the data for 17 Galactic GCs provided by T98 themselves, by definition in the T98 system. The original spectra were obtained by Burstein et al. (1984) with the image dissector scanner (IDS) at the 3m Shane Telescope of the Lick Observatory, and the absorption-line indices were re-measured by T98. Next, we incorporated the new data for 41 GCs from spectra obtained with the Blanco 4m telescope by Schiavon et al. (2005, hereafter S05)³. We have measured the needed indices (Mg2, Mgb,

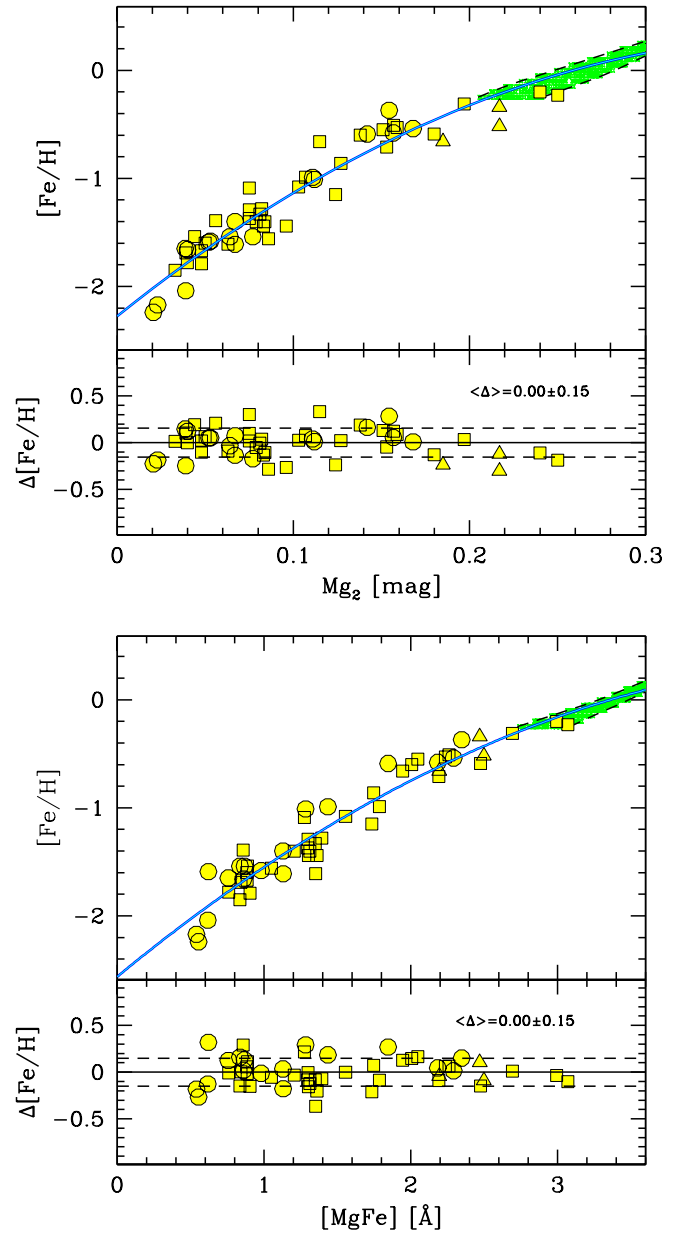


Fig. 3. The adopted calibrations for Mg2 and [MgFe] vs. [Fe/H] (continuum lines) are superposed to the accounted set of Galactic globular clusters from T98 (dots), S05 (squares), and B04 (triangles). The shaded regions at super-solar metallicity are the envelope of the theoretical predictions from several SSP models, as discussed in the text. A comparison between the empirical metallicities and ZW84 with the mean differences and rms are also reported in the lower panels. The dashed lines enclose the rms. The color figures are available in the electronic edition.

Fe5270 and Fe5335) from the Schiavon et al.'s spectra as described in detail in Section 3.1, below. We used the 8 clusters in common with the T98 to derive a simple least square fit converting indices from the S05 to the T98 system (using OLS(X|Y), according to Isobe et al. (1990); see Fig. 1). The derived values of the (*a*, *b*) coefficients for the various indices are reported in Table 1.

Indices for further 3 GCs were taken from Beasley et al. (2004) (hereafter B04) who re-measured Lick indices for 12 GCs

³ see <http://www.noao.edu/ggclib>.

spectra obtained by Cohen et al. (1998). The coefficients given in Table 2, derived by least-square fitting for clusters in common, as above, were used to convert the B04 indices into the T98 system. Fig. 2 compares the values of the indices from the sample obtained by joining the data from T98 and S05 with the B04 sample, after transformation to the T98 system. The plots show that the set of measures we have assembled is *very* homogeneous: any residual systematic and/or random scatter is of order of $\sim 5\%$ of the range spanned by the index, or smaller.

We merged all the sources described above into a global sample comprising 53 Galactic GCs with metallicities $-2.24 \leq [Fe/H] \leq -0.23$ in the ZW84 scale. In case of multiple measures we adopted one single source according to the following ranking: T98, S05 and B04. Lick indices, source and uncertainties for all sample adopted are given in Table 3.

As recalled in Sect. 1, it is known since long time that M31, as well as other giant galaxies (see Harris et al. 1992), hosts GCs that are significantly more metal rich than found in the Milky Way, possibly up to super-solar metallicities. To extend the range of applicability of our metallicity scale at the super solar regime - where we lack observed calibrators - we complemented our sample with a suitable set of several models for old SSPs (i.e. 12-12.5 Gyr, see Gratton et al. (1997)), with metallicity in the range $-0.3 \leq [Fe/H] \leq +0.5$. In particular, the theoretical predictions by Buzzoni (1989), Worthey (1994), Bruzual & Charlot (2003), Thomas et al. (2004), and Tantalo & Chiosi (2004b) have been considered. The simultaneous use of models from different authors provided a confident estimate of the internal uncertainty of the theoretical framework, intrinsic to the different input physics among the various theoretical synthesis codes. Therefore, to fit our calibrating relations we adopted a composite sample made by the empirical set of 53 Galactic GC in the range $-2.5 \leq [Fe/H] < -0.2$, plus the theoretically predicted index values described above, considered as observed points, in the range $-0.2 \leq [Fe/H] \leq +0.50$. While the agreement between the observed points and the models predictions is quite good over the whole metallicity range covered by Galactic GCs (see Fig. 5, below), the reader must be aware that the metallicity scale proposed here is not constrained by empirical calibrators in the solar and super-solar regime.

To avoid confusion resulting by plotting many different symbols in such a restricted range of metallicities, in Fig. 3 we simply plot a sketch of the envelope enclosing all the theoretical points that were considered in the calibration.

The two best-fit relations are shown in Fig. 3; they are the following second order polynomials represented by:

$$[Fe/H]_{[MgFe]} = -2.563 + 1.119[MgFe] - 0.106[MgFe]^2 \quad (1)$$

± 0.15 dex, r.m.s.

$$[Fe/H]_{Mg_2} = -2.276 + 13.053Mg_2 - 16.462Mg_2^2 \quad (2)$$

± 0.15 dex, r.m.s

Equations 1 and 2 are the fundamental calibrating relations of the proposed metallicity scale. When all the needed observables are available, the final metallicity value is obtained from Eq. 1; otherwise one shall recur to Eq. 2.

The internal consistency of the adopted scale is verified in Fig. 4, where the original metallicity values of the calibrating clusters are compared with those obtained with our calibrations. The r.m.s. scatter is $\simeq 0.15$ dex. Fig. 3 and Fig. 4 suggest that our

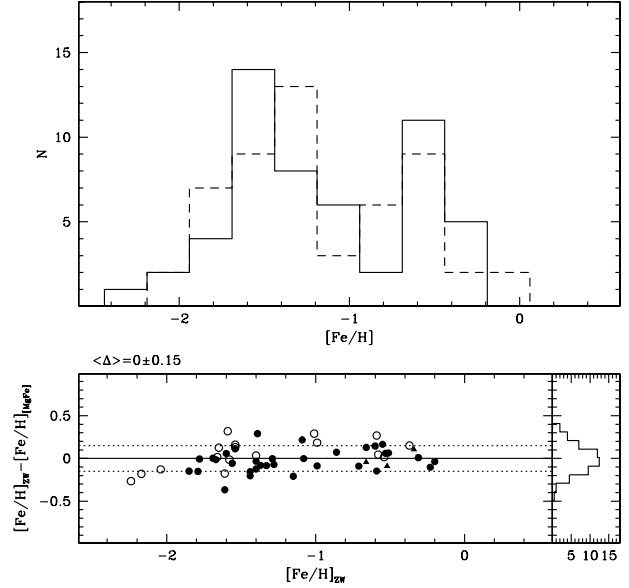


Fig. 4. *Upper Panel:* Comparison of the input MW GC metallicities from ZW84 and Armandroff & Zinn (1988) (continuous line) with those obtained from the empirical metallicity calibration (dashed line). *Lower Panels:* Comparison of the metallicity observed for Galactic globular clusters with the estimates from the $[MgFe]$ index. Open circles are Galactic globulars from T98, filled circle from S05 and triangles from B04. The dashed lines enclose the rms.

scale is less sensitive to metallicity variations and more uncertain at the metal-poor end, for $[Fe/H] \lesssim -1.9$. This is a general characteristic of scales based on integrated Lick indices (see, for example Faber et al. 1985; Cohen et al. 2003) and must be taken into account when very metal poor clusters are considered.

The effects of age assumptions are explored in Fig. 5, where we compare our Mg_2 data with an illustrative set of theoretical models from several population synthesis codes. In particular, we relied on the models by Buzzoni (1989, 1995a), Worthey et al. (1994), Girardi et al. (2000), Bruzual & Charlot (2003), Tantalo & Chiosi (2004b). The upper panel of the figure displays a collection of the 12 Gyr model predictions, while the expected shift in the theoretical loci when moving to ages younger is estimated in the lower panel. One can see that any change in age, say from 12 to 5 Gyr, reflects in a shallower slope of the theoretical $[Fe/H]$ vs. Mg_2 calibration, as a consequence of a larger offset ($\Delta Mg_2 \sim -0.05$ mag) at solar metallicity. On the other hand, any enhancement in the $[\alpha/Fe]$ element partition results in a (roughly) solid shift of the curve shelf to correspondingly lower values of $[Fe/H]$, as sketched on the plot.

The comparison between our empirical calibrating relations and the model predictions reveal that the application of our method to clusters as young as 5 Gyr, in the metallicity range $-2.0 < [Fe/H] < 0.0$, would lead to systematic errors in the estimated metallicity as small as ± 0.2 dex, i.e. of the same order of the typical statistical uncertainty. In any case, a good safety criterion would be to limit the application to clusters older than 7-8 Gyr.

Table 3. Lick indices for MW globular clusters. Indices were computed with the passband definitions of Trager et al. (1998) and were shifted in this system.

Cluster	Mg ₂ mag	eMg ₂ mag	Mgb Å	eMgb Å	Fe5270 Å	eFe5270 Å	Fe5335 Å	eFe5335 Å	Source ^a
NGC 104	0.153	0.007	3.022	0.013	1.925	0.015	1.256	0.017	2
NGC 1851	0.075	0.009	1.396	0.024	1.606	0.026	0.820	0.030	2
NGC 1904	0.039	0.009	0.788	0.035	1.297	0.039	0.516	0.046	2
NGC 2298	0.033	0.012	0.907	0.063	1.154	0.071	0.391	0.081	2
NGC 2808	0.075	0.007	1.374	0.015	1.613	0.017	0.838	0.019	2
NGC 3201	0.063	0.009	1.836	0.032	1.407	0.036	0.583	0.041	2
NGC 5024	0.039	0.010	0.830	0.295	0.370	0.268	0.550	0.281	1
NGC 5272	0.040	0.008	1.010	0.235	1.060	0.220	0.410	0.213	1
NGC 5286	0.048	0.009	0.903	0.023	1.287	0.026	0.526	0.030	2
NGC 5904	0.067	0.010	1.380	0.300	1.530	0.282	0.320	0.257	1
NGC 5927	0.197	0.009	3.885	0.035	2.183	0.039	1.549	0.044	2
NGC 5946	0.056	0.009	0.844	0.058	1.337	0.063	0.410	0.072	2
NGC 5986	0.048	0.009	0.900	0.026	1.278	0.029	0.465	0.034	2
NGC 6121	0.081	0.009	1.677	0.023	1.467	0.026	0.705	0.030	2
NGC 6171	0.111	0.015	1.800	0.447	1.710	0.420	0.580	0.427	1
NGC 6205	0.039	0.006	0.725	0.140	0.976	0.131	0.609	0.136	1
NGC 6218	0.067	0.011	1.360	0.338	1.380	0.317	0.500	0.316	1
NGC 6235	0.079	0.012	1.188	0.068	1.599	0.074	0.855	0.084	2
NGC 6254	0.050	0.009	0.861	0.023	1.315	0.026	0.495	0.029	2
NGC 6266	0.082	0.007	1.638	0.015	1.555	0.017	0.821	0.019	2
NGC 6284	0.084	0.009	1.562	0.037	1.475	0.041	0.730	0.047	2
NGC 6229	0.077	0.013	1.100	0.398	0.980	0.372	0.390	0.356	1
NGC 6304	0.180	0.009	3.545	0.035	2.056	0.039	1.399	0.044	2
NGC 6316	0.151	0.009	2.896	0.045	1.864	0.049	1.033	0.055	2
NGC 6333	0.040	0.009	0.748	0.028	1.213	0.032	0.336	0.036	2
NGC 6342	0.115	0.012	2.737	0.081	1.663	0.091	1.099	0.102	2
NGC 6352	0.157	0.009	3.198	0.044	1.867	0.049	1.329	0.056	2
NGC 6341	0.021	0.005	0.800	0.176	0.448	0.161	0.323	0.151	1
NGC 6356	0.168	0.009	3.060	0.251	2.034	0.236	1.400	0.263	1
NGC 6362	0.103	0.009	2.099	0.034	1.567	0.038	0.741	0.044	2
NGC 6388	0.138	0.007	2.393	0.017	2.029	0.018	1.335	0.021	2
NGC 6440	0.217	0.010	3.443	0.080	2.131	0.130	1.412	0.130	3
NGC 6441	0.159	0.009	2.921	0.020	2.043	0.022	1.383	0.025	2
NGC 6522	0.096	0.009	1.543	0.032	1.597	0.035	0.803	0.039	2
NGC 6528	0.250	0.009	4.377	0.042	2.421	0.046	1.884	0.051	2
NGC 6539	0.185	0.010	2.970	0.100	1.995	0.150	1.246	0.150	3
NGC 6544	0.086	0.009	0.950	0.046	1.564	0.049	0.764	0.055	2
NGC 6553	0.240	0.009	4.300	0.042	2.418	0.045	1.751	0.051	2
NGC 6569	0.127	0.009	2.329	0.049	1.654	0.054	0.967	0.061	2
NGC 6624	0.154	0.008	2.860	0.240	2.233	0.226	1.618	0.253	1
NGC 6626	0.083	0.009	1.554	0.025	1.445	0.027	0.743	0.031	2
NGC 6637	0.142	0.010	2.926	0.288	1.369	0.269	0.961	0.292	1
NGC 6638	0.124	0.009	2.184	0.035	1.736	0.038	1.021	0.043	2
NGC 6652	0.107	0.009	2.381	0.030	1.722	0.034	0.957	0.039	2
NGC 6712	0.112	0.015	1.570	0.431	1.410	0.405	0.690	0.423	1
NGC 6723	0.075	0.009	1.554	0.031	1.462	0.035	0.636	0.040	2
NGC 6752	0.044	0.009	0.924	0.025	1.264	0.029	0.445	0.033	2
NGC 6760	0.217	0.010	3.496	0.080	2.116	0.140	1.455	0.130	3
NGC 6838	0.157	0.010	2.628	0.295	1.774	0.277	1.855	0.314	1
NGC 6981	0.064	0.014	0.810	0.421	1.280	0.397	0.450	0.389	1
NGC 7006	0.052	0.012	0.665	0.352	0.529	0.326	0.633	0.344	1
NGC 7078	0.023	0.007	0.420	0.211	1.080	0.201	0.310	0.182	1
NGC 7089	0.053	0.008	0.900	0.242	1.260	0.228	0.880	0.245	1

^a Dataset label: 1 – Trager et al. (1998), 2 – Schiavon et al. (2005), 3 – Beasley et al. (2004).

3. The sample of M31 globular clusters

The M31 GCs Lick indices used in this study are taken from our observations and from several sources available in literature. In this section we describe the various data we adopted and how we transformed the different sets of measures into the T98 system.

In the following analysis we will consider only objects classified in the RBC as *genuine old M31 clusters*, i.e. having *classification flag* f=1. The possibility of contamination of the sample by spurious sources is discussed in Sect. 3.4, below.

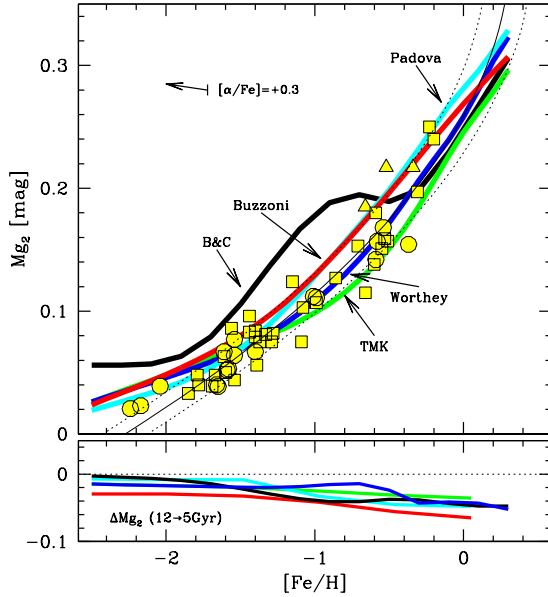


Fig. 5. (*upper panel*) - Mg_2 index distribution of the MW GCs (symbols are the same as Fig. 3) compared to the stellar population models of Buzzoni (1989, 1995a), Worthey et al. (1994), Girardi et al. (2000) (labelled as “Padova” on the plot), Bruzual & Charlot (2003) (“B&C”), Tantaló & Chiosi (2004b) (“TMK”). An age of 12 Gyr is assumed throughout, with solar $[\alpha/Fe]$ element partition. The thin line indicates the empirical calibration with its 1σ uncertainty. The effect of α -element enhancement is sketched by the arrow, for a change $[\alpha/Fe] = +0.3$. In the *lower panel* we assess on the contrary the effect of a change in age. For the same theoretical models we report the expected index variation (ΔMg_2) for a 5 Gyr stellar population along the full metallicity range. The color figure is available in the electronic edition.

3.1. Indices from our own spectra

First, we obtained new measures of Lick indices for the sample of M31 GCs described in Galleti et al. (2006a) and Galleti et al. (2007). The spectra were taken with the AF2/WYFFOS multi-fiber spectrograph at the 4.2m William Herschel telescope (WHT), with DoLoRes at the 3.5m Telescopio Nazionale Galileo (TNG), Roque de los Muchachos (La Palma, Spain), and with BFOSC at the Cassini 1.52m telescope of the Loiano Observatory (Bologna, Italy). The data acquisition, reduction and the resulting radial velocities (and membership) are fully described in Galleti et al. (2006a).

All the spectra were flux-calibrated, using various spectrophotometric standard stars to convert counts into flux units. We selected 88 confirmed clusters having the best spectra, i.e. $S/N \geq 15$, 69 from the WHT set, 14 from the TNG set and 5 from the Loiano set. During each observing night we also collected accurate ($S/N > 20$) observations of GCs in common with T98.

All the selected spectra span a wavelength range including indices from Fe4531 to Fe5406. Each spectrum was shifted to zero radial velocity. Before measuring indices, one has carefully to degrade spectra of higher resolution to the resolution of the Lick system. We strictly followed the approach of Worthey & Ottaviani (1997) and degraded our spectra to the wavelength-dependent Lick resolution ($\sim 11.5 \text{ \AA}$ at 4000 \AA ,

Table 4. Correction terms of the transformation to match the Lick system for WHT, Loiano and TNG data in the sense $I_{\text{Lick}} = I_{\text{measured}} + c$.

Index	c WHT	rms WHT	c Loi	rms Loi	c TNG	rms TNG
Mg2	0.015	0.022	0.018	0.015	-0.016	0.015
Mgb	0.000	0.588	-0.122	0.290	-0.333	0.399
Fe5270	-0.210	0.451	-0.148	0.504	-0.108	0.451
Fe5335	-0.230	0.346 ^a	-0.188	0.287	-0.188	0.218

^a We have not considered B178 in the fit for AF2/WYFFOS data.

8.4 \AA at 4900 \AA , and 9.8 \AA at 6000 \AA) with a variable-width Gaussian kernel.

The derived indices were then compared with those provided by T98 for 9, 14, and 10 clusters in common for the WHT, Loiano and TNG sets, respectively. It was found that all the considered indices can be reported into the T98 just by adding the constant values listed in Table 4. The comparison between the *corrected* values from the various sets and the measures by T98 are shown in Fig. 6. Our Lick index measurements and index uncertainties are listed in Appendix A, Table A.1. Errors were determined using photon statistics, following the formulae given in Cardiel et al. (1998). They do not incorporate the uncertainty due to our transformation to the Lick system, that is quantified by the r.m.s. scatter reported in Table 4.

3.2. Data from literature

To assemble as large as possible a dataset of metallicities in the new scale, we complemented the measures described above with other clusters for which there are published measures of the required Lick indices. In all cases we derived the equations to transform the published values into the T98 system using clusters in common between each considered set and T98, as done above for our measures. The following sources were adopted:

1. First, we have included the measures by T98 itself, that are available for 18 M31 globular clusters. These spectra were obtained by Burstein et al. (1984) with the image dissector scanner (IDS) at the 3m Shane Telescope of the Lick Observatory. The absorption-line indices are re-measured by T98 system and they define the standard-system.
2. Indices for 30 clusters have taken from Beasley et al. (2004) (B04), who obtained high S/N spectra ($S/N > 30 \text{ pixel}^{-1}$) with the Low Resolution Imaging Spectrograph (LRIS) on the Keck I telescope. The set of Lick line indices was measured with the passband definitions of Worthey et al. (1994) and was not corrected to the system of T98. However the three clusters in common with T98 show an excellent agreement with the standard system (see Fig 7).
3. We have incorporated the dataset of Puzia et al. (2005) (Pz05), who measured Lick indices, with the T98 definition, for 29 M31 GCs from the best spectra ($S/N > 25 \text{ per \AA}$) of the Perrett et al. (2002, hereafter P02) sample, obtained with the WYFOSS at the 4m WHT telescope.
4. We also have included the indices for further ~ 120 clusters, from the lower S/N spectra of the P02⁴ sample.

⁴ Private communication.

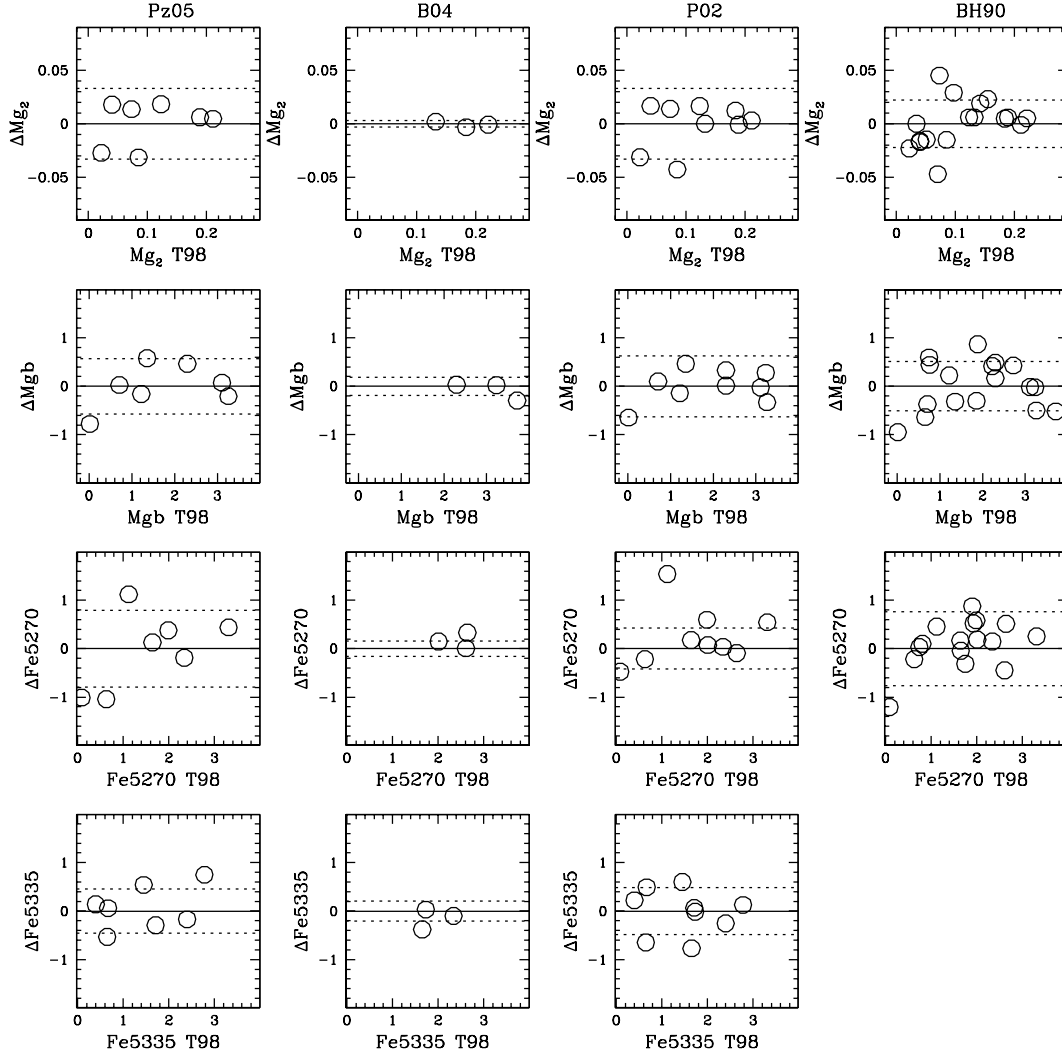


Fig. 7. A comparison of the common GCs between Trager and each sample after the shifts according to Table 5. Dashed lines show the rms.

Table 5. Coefficient for transformations to the Lick system of the literature data

Index	<i>a</i>	<i>c</i>	rms	<i>a</i>	<i>c</i>	rms	<i>a</i>	<i>c</i>	rms	<i>a</i>	<i>c</i>	rms
	Pz05			B04			P02			BH90		
Mg2	0.731	0.017	0.033	0.000	-0.020	0.003	0.730	0.070	0.033	0.000	0.015	0.022
Mgb	0.764	0.424	0.572	0.000	0.000	0.186	0.681	0.240	0.631 ^a	0.000	-0.27	0.508
Fe5270	0.000	0.000	0.790	0.000	0.000	0.161	0.000	-0.353	0.422 ^b	0.639	0.731	0.762
Fe5335	0.000	0.000	0.454	0.000	0.000	0.208	0.000	0.000	0.485			

^a we have not considered B015 in the fit data.

^b we have not considered B012 in the fit data.

The absorption-line indices were measured with the old passband definitions of Faber (1973) and Brodie & Hanes (1986). When needed, we converted the value of P02 to the

commonly used Å-scale for atomic indices⁵.

⁵ The transformation between wavelength and magnitude scale can be performed with the equations:

$$I_{\text{\AA}} = (\lambda_{\text{max}} - \lambda_{\text{min}})(1 - 10^{-0.4I_m}) \quad (3)$$

$$I_m = -2.5 \log[1 - (I_{\text{\AA}}/(\lambda_{\text{max}} - \lambda_{\text{min}}))] \quad (4)$$

where λ_{max} and λ_{min} define the red and blue boundaries of the feature passband.

5. The same procedure have applied to the Brodie & Huchra (1990) (BH90) data obtained with the Multiple Mirror Telescope (MMT). BH90 have measured ~ 150 absorption-line indices in their bandpass definitions from atmospheric cut-off at 3200Å to NaI, not including thus the Fe5335 index.

The various sets of indices (I_i) were transformed into the T98 system by the equation:

$$I_{T98} = I_i + aI_i + c$$

The coefficients of the adopted transformations are reported in Table 5, and the corrected indices are compared to the T98 values in Fig. 7.

The same procedure has been adopted to transform also the $H\beta$ index into the T98 system, when available. In all the considered cases, a constant shift appears to be an adequate transformation; the comparison of the corrected $H\beta$ values and the adopted shifts and r.m.s. are shown in Fig. 8.

3.3. Adopted metallicities

The indices transformed into the T98 system were used to compute the metallicities from Equations 1 and 2. In case of multiple measures of the same spectral index for a given GC, we always choose the value obtained from the spectrum with the highest S/N (when available) and/or with the smallest error. Individual indices estimates and the associated uncertainties for these datasets (296) are given in Appendix A, Table A.2.

Cluster metallicities and the associated uncertainties have been determined from Eq. 1 when possible, and from Mg2 in the other cases, i.e. when measures of Fe5270 and/or Fe5335 are lacking. Since the index–metallicity relation used is valid only for old globular clusters, (see Sect. 2), we have removed all possibly young objects. The empirical metallicities for 245 M31 GCs (see Sect. 3.4, below) are reported in Appendix A, Table A.3.

3.4. Possible contaminations

All the M31 clusters comprised in our analysis are class f=1 RBC entries; that is, they are all classified as genuine M31 members whose nature has been confirmed either spectroscopically and/or by means of high-resolution imaging (see Galleti et al. 2006a, for a detailed discussion about the classification of M31 GCs). While the sample should be largely dominated by bona-fide clusters, some spurious object may always be present as a truly final word on the nature of these objects can be obtained only by resolving them (at least partially) into individual stars by means of high resolution imaging. However, the recently published large spectroscopic and imaging survey by Caldwell et al. (2009) allows us to extensively check the classifications adopted in the RBC with fully independent and homogeneous data.

Of the 252 class f=1 clusters that we originally considered in our analysis, 247 were also observed and classified by Caldwell et al. (2009), and only *seven* of them, namely B025D, B026D, B043D, B046D, B215D, B248D and DAO25, were classified as non-clusters by these authors. For this reason, they have been excluded from our sample, reducing the total number of clusters with metallicity estimate from 252 to 245. Moreover, both B289D and B292D are suspected by Caldwell et al. (2009) to be in fact stars. Since these cases are not clear-cut, we mark these objects as potentially misclassified but we keep them in our globular cluster sample. Caldwell et al. (2009) *confirmed the RBC classification for all the remaining 238 clusters in common between the two samples*, i.e. all of them are classified

as genuine globulars. We stress that for the large majority of these clusters this classification has been previously confirmed also by other authors. Finally, of the five clusters of our sample that have not been observed by Caldwell et al. (2009), i.e. B514, MCGC1, MCGC8, MCGC10, and B344D, the first four have been confirmed as genuine old globulars from their HST CMDs (Galleti et al. 2006b; Mackey et al. 2007). Hence, according to the above cross-check, we conclude that before the exclusion of the seven objects re-classified by Caldwell et al. (2009) the contamination of our sample by non-clusters was $\lesssim 4\%$, and should be significantly lower than this in the final, cleaned sample.

As said in the Sect. 2.1, the derived calibrations are valid only for old GCs (age > 7 Gyr), hence it would be wise to exclude possibly young clusters from the final sample. The most widely used age indicators among Lick indices are the Balmer lines (see Fusi Pecci et al. 2005; Caldwell et al. 2009, and references therein). Here we adopt the $H\beta$ index to clean our sample from possibly young objects on an objective basis. In particular, we excluded since the beginning all the objects with $H\beta > 3.7$ Å (see Fusi Pecci et al. 2005, for a detailed discussion)⁶.

To investigate the problem in deeper detail we have checked any other cluster that has been suggested by some author as possibly young, irrespective of its $H\beta$ value. Of 245 clusters for which we have derived metallicities, there are 28 such clusters (see Fusi Pecci et al. 2005). Seven of these have published color-magnitude diagrams showing that they are very likely old GCs: B311, B358 and B468 by Rich et al. (2005), B008 by Perina et al. (2009), B083, B347 and NB16 by Perina et al. (2009b). Additional 16 clusters have been recently classified as old from their spectra by Caldwell et al. (2009, included in the cross-check described above), B015, B030, B047, B060, B070, B090, B117, B146, B154, B164, B197, B214, B232, B292, B328, B486. We did not find additional information for the remaining five (B018, B316, B431, B240D, DAO30): conservatively, we maintain them in the list of clusters for which we provide a metallicity estimate, but we exclude them from the cleaned sample used in the following analysis (Sect. 5).

In conclusion, the degree of contamination from any kind of spurious object (non-cluster or young cluster) in the sample considered in Sect. 5, should be extremely low. It should be recalled that the adopted selection in $H\beta$ would not exclude from our sample intermediate-age clusters ($2 \text{ Gyr} \lesssim \text{age} \lesssim 7 \text{ Gyr}$) that may be included with a wrong metallicity (lower than the true value). However these clusters should be quite rare in M31, if any, as among the several tens of M31 clusters having a CMD from HST, none has been found in that age range.

4. Comparisons with other sets of metallicities

In the following sections we compare our metallicity estimates for M31 globular clusters with those already available in the literature. We will discuss separately the comparison with (a) estimates obtained from empirical calibrations of spectral indices or colors, (b) estimates obtained from the fit of observed spectra with theoretical SPSS models, and (c) estimates obtained from the analysis of the Color Magnitude Diagrams of individual clusters (see Fusi Pecci et al. 1996; Holland et al.

⁶ In Fusi Pecci et al. (2005), to select clusters (possibly) younger than 2 Gyr the selection criteria $H\beta > 3.5$ Å was adopted, using $H\beta$ estimates from P02. However in the T98 system adopted here $H\beta_{T98} = H\beta_{P02} + 0.17$ Å (Fig. 8), hence the limit has been changed accordingly.

1997; Jablonka et al. 2000; Brown et al. 2004; Rich et al. 2005; Mackey et al. 2007; Perina et al. 2009, and references therein).

4.1. Comparison with $[Fe/H]$ from empirical calibrations

Before proceeding to with the compare our new scale with previous analysis, it is worth having a look at the degree of consistency between already existing sets. The comparison between H91 and P02 is particularly relevant in this context, as (a) they are the largest sets of empirical metallicities for M31 GCs available in the literature, (b) they should be consistent *by definition*, as P02 used the same definitions of the indices as H91 (see Brodie & Huchra 1990, hereafter BH90), and used metallicities by H91 for clusters in common between the two sets to calibrate $[Fe/H]$ vs. indices. To the original set of H91 we added the metallicities for further 35 M31 GCs obtained by Barmby et al. (2000) with the same method and strictly in the same system as H91.

Fig. 9 left panel reveals that there is a considerable scatter between the H91 and P02 sets of measures: the r.m.s. is 0.34 dex but differences up to ~ 1 dex are also present. This can be taken as a reference of the typical degree of agreement between independent sets. In the right panel we compare the P02 metallicities with those Pz05 where the dataset is the same. A large spread is also evident in this case.

It is important to recall here that to obtain the metallicity of M31 GCs from line indices, BH90 and H91 calibrated a relation between $[Fe/H]$ and the infrared colors $((V-K), (J-K))$ using Galactic GCs. Then, they used the infrared photometry of 40 M31 GCs by Frogel et al. (1980) and Bonoli et al. (1987) to obtain their metallicity from that relation, and merged this sample with i) a sample of Galactic GCs for which they measured the same line indices, and ii) with the average of the indices measured in several individual stars in the open cluster NGC188, that was adopted as a template for solar metallicity populations lacking among MW globulars. They used the merged sample to calibrate various indices against $[Fe/H]$. Finally, they used the relations to obtain a metallicity estimate for each index, and they adopted the weighted average of the values obtained from the various indices as their final metallicity estimate (H91). The complex procedure outlined above was dictated by the requirement to obtain the largest possible sample from the data available at the time, and to average out the errors by using the information from all the available indicators. On the other hand, our aim is to provide a clean and easily repeatable process to obtain metallicities from few selected spectral indices, as it is nowadays relatively easy to obtain high S/N spectra for most M31 GCs with 4m telescopes, and the 10m class telescopes are entering the game.

Fig. 10 shows that the difference between our metallicity estimates and those from H91 and P02 presents a scatter of the same amplitude as that existing between H91 and P02. Moreover, metallicities from our scale are systematically larger by up to ~ 0.3 dex for $[Fe/H] \gtrsim -1.4$ and systematically smaller for $[Fe/H] \lesssim -2.0$. Fig. 10 provides a strong warning on the reliability of empirical metallicity scales based on Lick indices from integrated spectra. While our metallicities and those by H91 and P02 present strong correlations, estimates for individual clusters can well differ by as much as ± 0.5 dex (or more) because of statistic or systematic effects. This is the fundamental reason that convinced us to avoid assembling metallicities from different sources for the RBC, trying instead to reach the maximum degree of homogeneity at the “index level” (Sect. 2 and 3) and the highest degree of internal consistency by converting the indices into metallicity with the same calibrating relations. The choice

of using just the Mg_2 , Mgb , $Fe5270$ and $Fe5335$ indices is also intended to minimize the effects on the final metallicity estimate of variations/anomalies in the abundance of other elements, like for instance C, N etc., or age effects, that may affect other indices (see, for example, Burstein et al. (2004), Fusi Pecci et al. (2005) and references therein). It is worth noting, in this context, that we have no particular a-posteriori reason to claim that our scale is *superior* to other existing empirical scales based on spectra. 2, we feel that we have made all the possible efforts to construct a very homogeneous and internally consistent scale for the RBC, designed for the easy and safe inclusion of any new set of indices that will be published in the future⁷.

Finally, Fig. 11 shows the comparison between our metallicities and those obtained from $(V-K)_0$ colors, using the calibrations by Barmby et al. (2000), taking the V-K colors from the RBC, and adopting two different sets of reddening estimates, i.e. those from Barmby et al. (2000)⁸ and from Fan et al. (2008). This comparison reveals the critical role of the (uncertain) reddening estimates on any metallicity scale based on colors: the two sets considered here differ only in the adopted reddening, yet the r.m.s scatter in the final metallicity is as large as ± 0.30 dex. The overall behavior in comparison with our scale is relatively similar to that of the H91 and P02 sets. This may be due to the fact that at the origin of these scales there is also a calibration of metallicity vs. integrated $(V-K)_0$ colors.

It is interesting to note that, independently of the adopted set of reddening, the metallicities obtained from $(V-K)_0$ are systematically lower than our spectroscopic estimates by a large amount, i.e. ≈ 0.4 dex, in average. We do not have a straightforward explanation for this remarkable systematic difference, we can just put forward some hypothesis for its origin. The observed effect can arise if the reddening values are systematically overestimated: using the $[Fe/H] - (V-K)_0$ calibration by Barmby et al. (2000) and assuming $E(V-K) = 2.75E(B-V)$, according to Cardelli et al. (1989), an overestimate of $E(B-V)$ by 0.09, in average, is sufficient to account for the whole 0.4 dex difference between the metallicity scales. While the required systematic in $E(B-V)$ is probably too large to be realistic, an overestimate of the reddening may provide a relevant (possibly the largest) contribution to the observed systematic difference in the metallicity. Systematic differences in the age distribution and/or in the abundance pattern between MW and M31 globulars can also contribute to the effect. In particular, Fig. 9 of Barmby et al. (2000) seems to suggest that the clusters of the two galaxies may not share the same $[Fe/H] - (V-K)_0$ relation.

4.2. Comparison with $[Fe/H]$ from SED fitting

We compare the metallicities of the M31 clusters derived from our empirical calibrations with those derived from SSP model fitting by Puzia et al. (2005) and Beasley et al. (2005) (using the TMB models) in Fig. 12. The model report the metallicities in $[Z/H]$ scale and a transformation to $[Fe/H]$ has been done through the equation: $[Fe/H] = [Z/H] - 0.94[\alpha/Fe]$ taken from Thomas et al. (2003, see also Trager et al. 2000). The clusters with derived age < 8 Gyr are excluded because our empirical calibrations are valid only for old GCs. To first order, the agreement between the literature values and the metallicities from our empirical relations is clearly satisfactory with B05, and acceptable

⁷ This will be possible a the condition that the considered set of indices have a sufficient number of clusters in common with our sample to obtain a good transformation of the indices into the T98 system

⁸ Private communication.

with Pz05, as shown in Fig. 12. The two sets of measures show systematics of opposite sign with respect to our scale: B05 finds values slightly lower than ours (by ~ 0.1 dex), Pz05 estimates are larger by ~ 0.2 dex, on average. It may be worthwhile to check if part of these differences may be due to the fact that these authors consider separately the metallicity from Iron peaks elements and the abundance of α elements, while our scale neglects this potentially relevant discrimination⁹.

Fig. 13 shows that this may be the case for B05: if our $[\text{Fe}/\text{H}]$ estimates are compared with B05 estimates of $[\text{Z}/\text{H}]$ the offset is reduced to zero and even the r.m.s. scatter is slightly reduced (having excluded the outlier B328). On the other hand the comparison with $[\text{Z}/\text{H}]$ exacerbates the systematic difference with Pz05, while significantly reducing the r.m.s. scatter. In conclusion, our new metallicity scale seems in much better agreement with scales derived from the detailed fitting of spectra with SPSS models than with other empirical scales.

4.3. Comparison with $[\text{Fe}/\text{H}]$ from CMDs

The estimates that can be obtained from CMDs of individual clusters by comparing the observed Red Giant Branch (RGB) with the RGB templates of well studied Galactic GCs probably provides one of the most reliable metallicities currently available for M31 GCs, of course under the hypothesis that the basic properties of the two GC systems are the same. For clusters that are not too compact and are not immersed in exceedingly crowded fields, HST photometry (either from the WFPC2, e.g. Rich et al. (2005), or the ACS, e.g. see Galleti et al. (2006b) and Mackey et al. (2007)) can provide clean and well defined CMDs of the RGB. In addition the Horizontal Branch morphology and the lack of bright Main Sequence stars give the best sanity check on the actual age of the cluster that can be currently achieved (see, in particular Brown et al. (2004)). Therefore, the comparison of our estimates with those obtained from good CMDs from HST is a compelling test of the reliability and accuracy of our new metallicity scale.

We collected metallicity from CMDs for 35 clusters in common with our list, from the following sources: Rich et al. (2005), that comprise the largest sample of published CMD of M31 GCs; Jablonka et al. (2000) that analyzed three GC in the bulge of M31; Brown et al. (2004), that studied in great detail B379; Galleti et al. (2006b) and Mackey et al. (2007) that considered clusters located in the outskirts of the galaxy and Perina et al. (2009). The comparison between our estimates and those obtained from the CMDs is presented in Fig. 14. The agreement is quite satisfying over the whole considered range. However, there is a small systematic offset between the metallicity estimates obtained from the spectra or from the CMDs, in the sense that the former are larger than the latter by ~ 0.1 dex, in average. This points to a real difference between the two independent scales, possibly related to how $[\alpha/\text{Fe}]$ is included in the two calibrations. We take the r.m.s. of the difference computed over the whole sample as the typical accuracy of our metallicity estimates (± 0.25 dex).

⁹ It is important to recall that our scale is not expected to strictly trace the abundance of *Iron*. In fact it is based on the ZW84 scale that, in turn, is based on the metallicities derived by Cohen (1983) from lines of various elements, including Mg (see Mendel et al. 2007, for a detailed discussion and references). Therefore it is likely a better proxy for the *total* metallicity than for the actual Iron abundance.

5. Discussion and Conclusions

Using our own data as well as datasets available in the literature, we have established a new homogeneous metallicity scale for M31 GCs. The scale is based on the Lick index Mg2 and on the combination of Mgb and Fe indices $[\text{MgFe}]$, that have been calibrated against well studied Galactic globulars (for $[\text{Fe}/\text{H}] < -0.2$) and a variety of old-age SSP theoretical models for $-0.2 \leq [\text{Fe}/\text{H}] \leq 0.50$. Our scale has been shown to be self-consistent within ± 0.25 dex, and it should be applied only to classical, old globular clusters.

In the following we briefly describe a few natural applications of the newly derived metallicity scale. In particular, (a) we derive and discuss the metallicity distribution of M31 GCs, (b) we explore the correlations between metallicity and kinematics, for the sample of 240 bona-fide old GCs described in Sect. 3.4, above.

5.1. Metallicity distribution

In Fig. 15 the Metallicity Distribution (MD) of our sample of M31 GCs is compared with its Milky Way counterpart.

The highest peak in the M31 MD occurs at $[\text{Fe}/\text{H}] \sim -0.9$, coinciding with the overall average of the sample $\langle [\text{Fe}/\text{H}] \rangle = -0.94$, significantly more metal rich than in the MW case, where the maximum is at $[\text{Fe}/\text{H}] \sim -1.5$ and the overall mean is $\langle [\text{Fe}/\text{H}] \rangle = -1.30$ (based on data from Harris 1996, that are in the ZW84 scale). The M31 system appears also to have a much larger fraction of clusters having $[\text{Fe}/\text{H}] > -0.5$ (23% of the total sample) with respect to the Milky Way (7%). It should be considered that the individual metallicity estimates for M31 clusters have much larger uncertainties with respect to their MW counterparts and this may produce some spurious widening of the MD for M31. However the shape of the distribution is essentially unchanged if we limit the analysis to the subset of clusters having errors in metallicity lower than ± 0.3 dex (132 clusters; dotted histogram in the upper panel of Fig. 15). Fig. 16 shows that the difference between the MDs of the two galaxies cannot be ascribed to spurious effects due to our calibration, as it can be re-conducted to genuine differences in the observable $[\text{MgFe}]$.

The MD of M31 GCs do not present any obvious structure like the bimodality encountered in the GC system of the Milky Way. Nevertheless the distribution for M31 clusters does not seem to be well represented by a single Gaussian distribution. Note that large errors on individual metallicities should contribute to wipe out real structures, not to produce spurious ones. The hypothesis of a multimodal underlying distribution has been compared with a unimodal representation using the parametric KMM test (Ashman et al. 1994), that compares the fits to the MD made with one or more Gaussian distributions. A two component model with modes at $[\text{Fe}/\text{H}] = -1.54$ and $[\text{Fe}/\text{H}] = -0.64$ is preferred to the unimodal case at the 99.1% confidence level (homoscedastic case) and at the 98.7% c.l. in the heteroscedastic case with peaks at $[\text{Fe}/\text{H}] = -1.79$ and $[\text{Fe}/\text{H}] = -0.76$. A three component model with modes at $[\text{Fe}/\text{H}] = -0.25$, -0.89 and -1.72 is also preferable to the unimodal one (99.8% c.l., in the homoscedastic case, and 99.6% c.l., in the heteroscedastic case with peaks at $[\text{Fe}/\text{H}] = -1.77$, $[\text{Fe}/\text{H}] = -0.80$ and $[\text{Fe}/\text{H}] = -0.01$), and nearly equivalent to the bimodal representation, from a statistical point of view. The preference of bi- and three- modal models over the unimodal case remains even if we consider the subset of clusters with the lowest metallicity errors described above. While clearly not conclusive, the above analysis suggests that there may be real structures in the MD of M31 globular

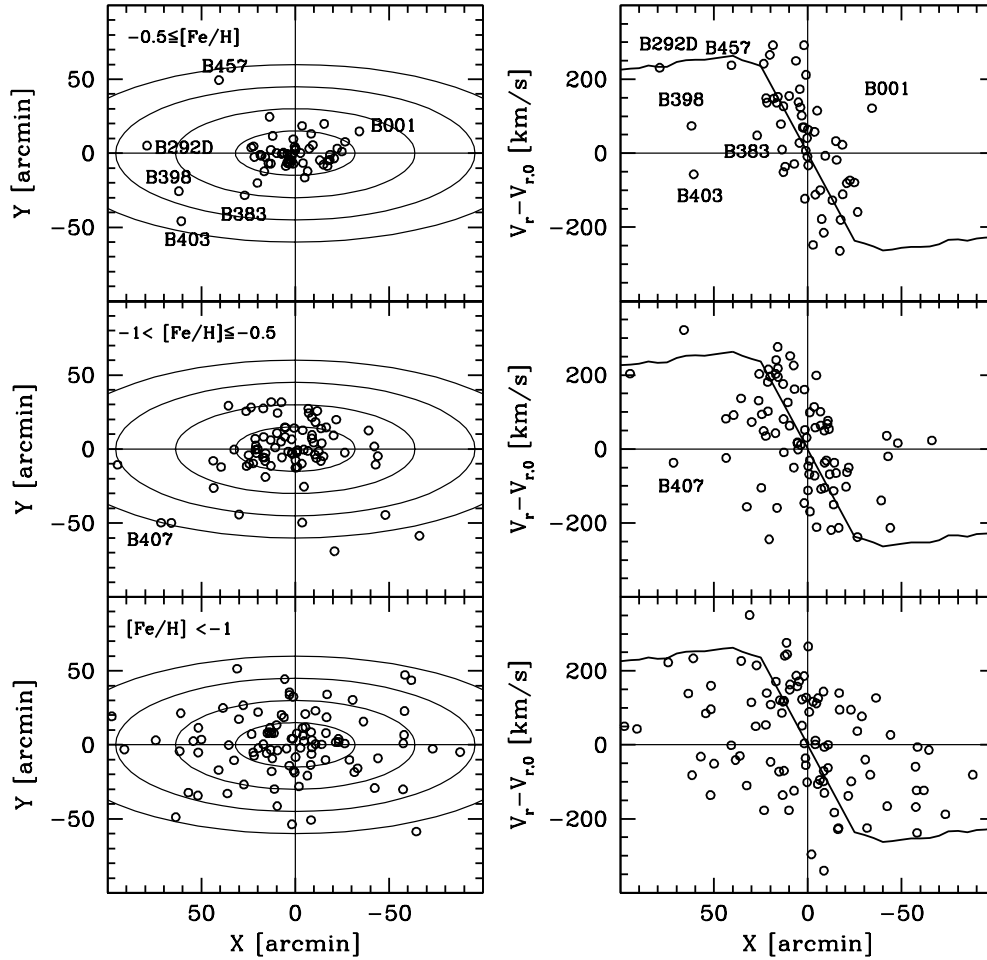


Fig. 17. Left Panels: Spatial distribution of three metallicity groups GCs in M31. The ellipses have a semimajor axis of 15, 30, 45, 60 arcmin. Right Panels: Radial velocities vs. the projected distances along the major axis (X). The solid line shows a HI rotation curve from Carignan et al. (2006).

clusters, in good agreement with the conclusions reached by Barmby et al. (2000), P02, Pz05, Fan et al. (2008) and Lee et al. (2008).

5.2. Metallicity and kinematics

Fig. 17 shows the positional and kinematical properties of M31 GCs divided into three groups according to their metallicity, i.e. a Metal Poor (MP) group ($[Fe/H] \leq -1.0$), a Metal Intermediate (MI) group ($-1.0 < [Fe/H] < -0.5$), and a Metal Rich (MR) group ($[Fe/H] \geq -0.5$). The left panels of Fig. 17 show the spatial distribution of the considered clusters in the canonical X,Y projected coordinate system (see Galleti et al. 2004, and references therein), with X along the major axis of the galaxy. In the right panels the radial velocity of the clusters (in the reference frame of M31) is plotted versus the X coordinate and compared with the rotation curve of the HI disk from Carignan et al. (2006).

It results quite clear from the inspection of Fig. 17 that the MR and MI subsamples display a significant rotation pattern, much similar to the rotation curve of neutral Hydrogen disk of M31. The MR clusters are more densely packed near the center

of the galaxy and appear to follow more closely the HI curve, whereas the MI clusters display a larger dispersion. MR clusters are likely associated with the prominent Bulge of M31.

The MP clusters show a much larger velocity dispersion at any distance from the center of the galaxy; in spite of that, they follow a significant rotation pattern in the same sense as the other clusters. Dividing the MP sample at $X=0$, we find (M31-centric) average velocities of $\langle V_{M31} \rangle = +59$ km/s and $\langle V_{M31} \rangle = -48$ km/s for the clusters with $X > 0$ and $X < 0$, respectively; the difference in the median velocities is even larger, as $V_{M31}^{med} = +86$ km/s and $V_{M31}^{med} = -59$ km/s, for the two subsets. Finally if the V_{M31} distributions of the $X > 0$ and $X < 0$ MP clusters are compared with a Kolmogorov-Smirnov test, it turns out that the probability that the two samples are drawn from the same distribution of V_{M31} is just 0.2%. In Sect. 3.4 we have shown that our sample should be reasonably clean from spurious sources (as for instance young massive clusters, that may be misclassified as metal-poor GCs and would follow the rotation pattern of the thin disk they belong to, see Fusi Pecci et al. 2005), hence we conclude that the rotation pattern of MP clusters is probably real. However an ultimate conclusion on this (relevant) issue could be achieved only when the actual nature of a significant subsam-

ple of MP clusters will be confirmed beyond any doubt from the CMD of their individual stars.

The above results are in good agreement with what previously found by P02 and Lee et al. (2008), among others. A more detailed discussion of these correlations between kinematics and metallicity is beyond the scope of the present paper. We address the interested reader to the thorough discussion by Lee et al. (2008). Here we just want to draw the attention of the reader on five of the six MR clusters lying at $R > 30'$ (labeled in Fig. 17). B001, B398 and B403 show no correlation with the overall rotation pattern. On the other hand B292D, and B457 lie straight on the flat branch of the HI rotation curve in spite of the fact that they are more than ~ 7 kpc away from all the other MR clusters (except B398 and B403, of course). These five objects clearly deserve new observations with high S/N spectra to verify both their metallicity and their radial velocity. If confirmed, their odd positions and kinematics would require an interpretation. Moreover, B403 and B407 (labeled in the MI panel of Fig. 17, and having $[Fe/H] = -0.65 \pm 0.15$) have very similar position and velocity (differing by ~ 20 km/s). The case of these two relatively metal-rich clusters in the outer halo of M31 is discussed in more detail in Perina et al. (2009).¹⁰

Acknowledgements. M.B. acknowledge the financial support of INAF through the PRIN2007 grant CRA 1.06.10.04. We are very grateful to P. Barmby and K. Perrett for providing their unpublished data for M31 GCs. This research has made use of NASA's Astrophysics Data System Bibliographic Services. We would like to thank the anonymous referee for their careful reading of the manuscript and helpful comments.

References

- Armandroff, T. E., & Zinn, R. 1988, *AJ*, 96, 92
- Ashman, K. M., Bird, C. M., & Zepf, S. E. 1994, *AJ*, 108, 2348
- Barmby, P., Huchra, J.P., Brodie, J.P., Forbes, D.A., Schroder, L.L., & Grillmair, C.J. 2000, *AJ*, 119, 727 [B00]
- Beasley, M.A., Brodie, J.P., Strader, J., Forbes, D.A., Proctor, R.N., Barmby, P., Huchra, J.P., 2004, *AJ*, 128, 1623 [B04]
- Beasley, M.A., Brodie, J.P., Strader, J., Forbes, D.A., Proctor, R.N., Barmby, P., Huchra, J.P., 2005, *AJ*, 129, 1412
- Bonoli, F., Delpino, F., Federici, L., & Fusi Pecci, F. 1987, *A&A*, 185, 25
- Brodie, J.P., Hanes, D.A. 1986, *ApJ*, 300, 258
- Brodie, J.P., Huchra, J.P. 1990, *ApJ*, 362, 503 [BH90]
- Brodie, J.P., Huchra, J.P., 1991, *ApJ*, 379, 157
- Brodie, J. P., & Strader, J. 2006, *ARA&A*, 44, 193
- Brown, T. M., Ferguson, H. C., Smith, E., Kimble, R. A., Sweigart, A. V., Renzini, A., Rich, R. M., & VandenBerg, D. A. 2004, *ApJ*, 613, L125
- Bruzual, G., Charlot, S. 2003, *MNRAS*, 344, 1000 [BC03]
- Burstein, D., Faber, S.M., Gaskell, C.M., Krumm, N. 1984, *ApJ*, 287, 586
- Burstein, D., Li, Y., Freeman, K.C., et al. 2004, *ApJ*, 614, 158
- Buzzoni, A. 1989, *ApJs*, 71, 817 (see also: <http://www.bo.astro.it/~eps/home.html> for the latest model update)
- Buzzoni, A., Gariboldi, G., & Mantegazza, L. 1992, *AJ*, 103, 1814
- Buzzoni, A., Mantegazza, L. & Gariboldi, G. 1994, *AJ*, 107, 513
- Buzzoni, A. 1995a, *ApJs*, 98, 69
- Buzzoni, A. 1995b in *Fresh views of elliptical galaxies*, ASP Conf. Ser., Vol. 86, eds. A. Buzzoni, A. Renzini & A. Serrano (San Francisco: ASP), p. 189
- Caldwell, N., Caldwell, N., Harding, P., Morrison, H., Rose, J. A., Schiavon, R., & Kriessler, J. 2009, *AJ*, 137, 94
- Cardelli, J.A., Clayton, G.C., & Mathis, J.S., 1989, *ApJ*, 345, 245
- Cardiel, N., Gorgas, J., Cenarro, J., & Gonzalez, J. J. 1998, *A&AS*, 127, 597
- Carignan, C., Chemin, L., Huchtmeier, W. K., & Lockman, F. J. 2006, *ApJ*, 641, L109
- Carretta, E., & Gratton, R. G. 1997, *A&AS*, 121, 95
- Carretta, E., Bragaglia, A., Gratton, R., & Lucatello, S., 2008, in *Chemical Evolution of Dwarf Galaxies and Stellar Clusters*, (arXiv:0811.3591)
- Cohen J. G., 1983, *ApJ*, 270, 654
- Cohen, J.G., Blakeslee, J.P. & Ryzhov, A. 1998, *ApJ*, 496, 808
- Cohen, J. G., Blakeslee, J. P., & Côté, P. 2003, *ApJ*, 592, 866 s
- Colucci, J.E., Bernstein, R.A., Cameron, S., McWilliam, A., & Cohen, J., 2009, *ApJ*, 704, 385
- Faber, S. M., 1973, *ApJ*, 179, 731
- Faber, S. M., Friel, E. D., Burstein, D., Gaskell, C. M. 1985, *ApJs*, 57, 711
- Fan, Z., Ma, J., de Grijs, R., & Zhou, X. 2008, *MNRAS*, 385, 1973
- Frogel, J.A., Persson, S.E., & Cohen, J.G. 1980, *ApJ*, 240, 785
- Fusi Pecci, F., Buonanno, R., Cacciari, C., Corsi, C. E., Djorgovski, S. G., Federici, L., Ferraro, F. R., Parmeggiani, G., & Rich, R. M. 1996, *AJ*, 112, 1461
- Fusi Pecci, F., Bellazzini, M., Buzzoni, A., De Simone, E., Federici, L., Galleti, S., 2005, *AJ*, 130, 554
- Galleti, S., Federici, L., Bellazzini, M., Fusi Pecci, F., Macrina, S., 2004, *A&A*, 416, 917
- Galleti, S., Federici, L., Bellazzini, M., Buzzoni, A., Fusi Pecci, F., 2006a, *A&A*, 456, 985
- Galleti, S., Federici, L., Bellazzini, M., Buzzoni, A., Fusi Pecci, F., 2006b, *ApJ*, 650, L107
- Galleti, S., Bellazzini, M., Federici, L., Buzzoni, A., & Fusi Pecci, F. 2007, *A&A*, 471, 127
- Girardi, L., Bressan, A., Bertelli, G., & Chiosi, C. 2000, *A&A*, 354, 892
- González, J. J. 1993, Ph.D. Thesis,
- Gratton, R. G., Fusi Pecci, F., Carretta, E., Clementini, G., Corsi, C. E., & Lattanzi, M. 1997, *ApJ*, 491, 749
- Gratton, R., Sneden, C., & Carretta, E., 2004, *ARA&A*, 42, 385
- Harris, W.E. 1996, *AJ*, 112, 1487 (see also: <http://physwww.physics.mcmaster.ca/~harris/mwgc.dat> for catalog update February 2003)
- Harris, G. L. H., Geisler, D., Harris, H. C., & Hesser, J. E. 1992, *AJ*, 104, 613
- Holland, S., Fahlman, G. G., & Richer, H. B. 1997, *AJ*, 114, 1488
- Huchra, J.P., Brodie, J.P., & Kent, S. 1991, *ApJ*, 370, 495 [H91]
- Ibata, R., Martin, N.F., Irwin, M.J., Chapman, S., Ferguson, A.M.N., Lewis, G.F., & McConnachie, A. W., 2007, *ApJ*, 671, 1591
- Isobe, T., Feigelson, E. D., Akritas, M. G., & Babu, G. J. 1990, *ApJ*, 364, 104
- Jablonska, P., Courbin, F., Meylan, G., Sarajedini, A., Bridges, T. J., Magain, P., 2000, *A&A*, 359, 131
- Lee, M. G., Hwang, H. S., Kim, S. C., Park, H. S., Geisler, D., Sarajedini, A., & Harris, W. E. 2008, *ApJ*, 674, 886
- MacArthur, L. A. 2005, *ApJ*, 623, 795
- Mackey, A. D., Huxor, A., Ferguson, A.M.N., Tanvir, N.R., Irwin, M., Ibata, R., Bridges, T., Johnson, R.A. & Lewis, G. 2007, *ApJ*, 655, L85
- Mackey, A. D., et al., 2009, *MNRAS*, in press (arXiv:0909.1456)
- McWilliam, A., 1997, *ARA&A*, 35, 503
- Mendel, J. T., Proctor, R. N., & Forbes, D. A. 2007, *MNRAS*, 379, 1618
- Perrett, K.M., Bridges, T.J., Hanes, D.A., et al. 2002, *AJ*, 123, 2490 [P02]
- Perina, S., et al. 2009, submitted to *A&A*
- Perina, S., et al. 2009b, in preparation
- Press, W. H., Teukolsky, S. A., Vetterling, W. T & Flannery, B., B 1992, *Numerical Recipes in FORTRAN*, Second edition
- Pritzl, B. J., Venn, K. A., & Irwin, M. 2005, *AJ*, 130, 2140
- Puzia, T.H., Perrett, K.M., Bridges, T.J., 2005, *A&A*, 434, 909 [Pz05]
- Renzini, A., & Fusi Pecci, F. 1988, *ARAA*, 26, 199 [RFP88]
- Renzini, A., & Buzzoni, A., 1986, in *Spectral evolution of galaxies*, Dordrecht, D. Reidel Publishing Co., p. 195
- Rich R.M., Corsi C.E., Cacciari C., Federici L., Fusi Pecci F., Djorgovski S.G., Freedman, W. L., 2005, *AJ*, 129, 2670
- Schiavon, R. P., Rose, J. A., Courteau, S., & MacArthur, L. A. 2005, *ApJS*, 160, 163 [S05]
- Schlegel, D. J., Finkbeiner, D. P., & Davis, M. 1998, *ApJ*, 500, 525
- Sneden, C. 2005, *IAU Symposium*, 228, 337
- Tantalo, R., & Chiosi, C. 2004, *MNRAS*, 353, 405
- Tantalo, R., & Chiosi, C. 2004, *MNRAS*, 353, 917
- Thomas, D., Maraston, C., Korn, A. 2004, *MNRAS*, 351, 19
- Thomas, D., Maraston, C., & Bender, R. 2003, *MNRAS*, 339, 897 [TMB]

¹⁰ *Note Added in Proofs:* After the acceptance of the present paper, a work appeared presenting metallicities of a few M31 GCs from high resolution integrated spectra (Colucci et al. 2009). It is interesting to note that for four of the five clusters in common, our $[Fe/H]$ estimates agree with those of Colucci et al. (2009) to within < 0.1 dex. Our estimate for the fifth cluster (B358, which is in the deep metal-poor regime in which our observable are less sensitive to metallicity, see Sect. 2, above) is 0.36 dex higher than what found by Colucci et al. (2009), i.e. $[Fe/H] = -1.85 \pm 0.19$ vs. $[Fe/H] = -2.21 \pm 0.03$; however the difference is less than 2σ . It appears that our own scale and that based on high-resolution spectroscopy introduced by these authors are in excellent agreement. We note also that our metallicity estimate for the remote M31 cluster MGC1, $[Fe/H] = -2.16 \pm 0.28$, is in excellent agreement with what recently obtained by Mackey et al. (2009) from a high-quality CMD, $[M/H] \approx -2.3$.

- Trager, S.C., Worthey, G., Faber, S.M., Burstein, D., & González, J.J. 1998, ApJS, 116, 1 [T98]
Trager, S. C., Faber, S. M., Worthey, G., & González, J. J. 2000, AJ, 119, 1645
van den Bergh, S. 1969, ApJs, 19, 145
Worthey, G. 1994, ApJs, 95, 107
Worthey, G. 1996, ASPC, 98, 467
Worthey, G., Faber, S. M., Gonzalez, J. J., & Burstein, D. 1994, ApJS, 94, 687
Worthey, G., & Ottaviani, D. L. 1997, ApJS, 111, 377
Zinn, R., & West, M. J. 1984, ApJS, 55, 45 [ZW84]
Zinn, R. 1985, ApJ 293, 424

Appendix A: Homogeneous Lick indices in the T98 system for M31 globular clusters

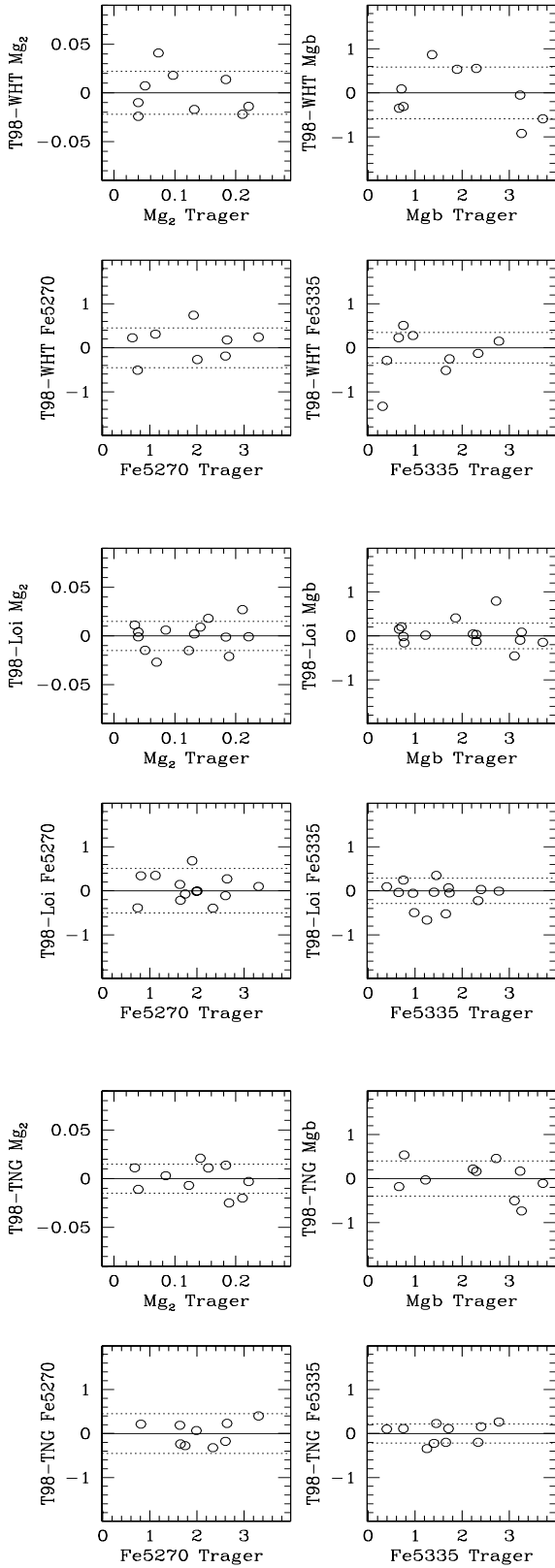


Fig. 6. Comparison of Lick indices measurements from WHT, Loiano, TNG after transformation and T98, for the clusters in common. The dotted lines enclose the range of the rms. In AF2/WYFFOS data for Fe5335 we have not considered B178 in the fit data. In Loiano and TNG data we have not considered B193.

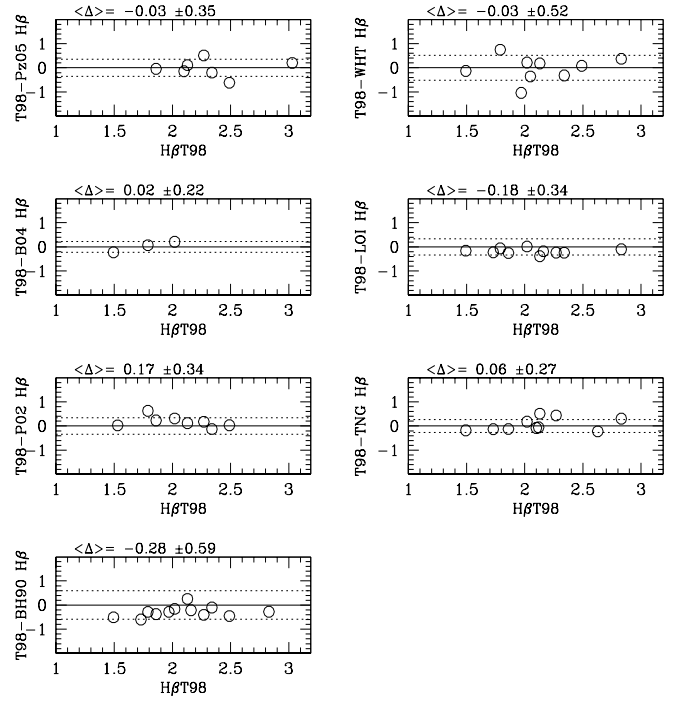


Fig. 8. A comparison of the $H\beta$ index measurements in common with T98. The mean differences and rms are also reported. The dashed lines enclose the rms.

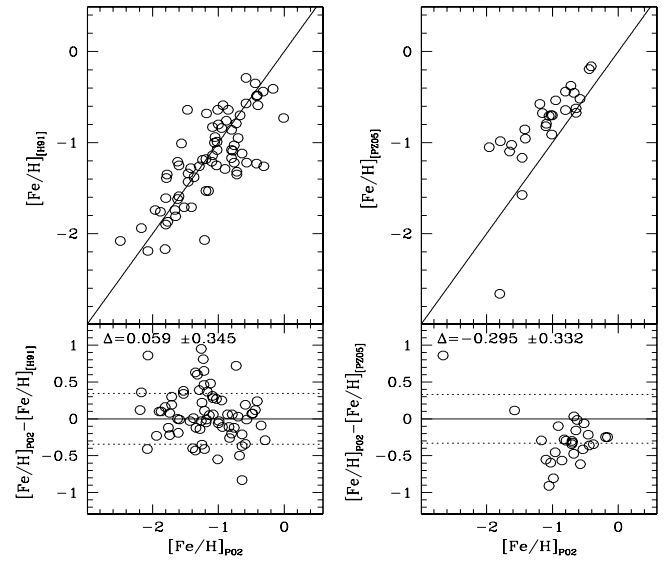


Fig. 9. Comparison of the metallicities from P02 with H91 and B00 in the left panel and from P02 with PZ05 in the right panel. The solid line indicates the one-to-one relation. The dotted lines in the lower panel mark the σ value.

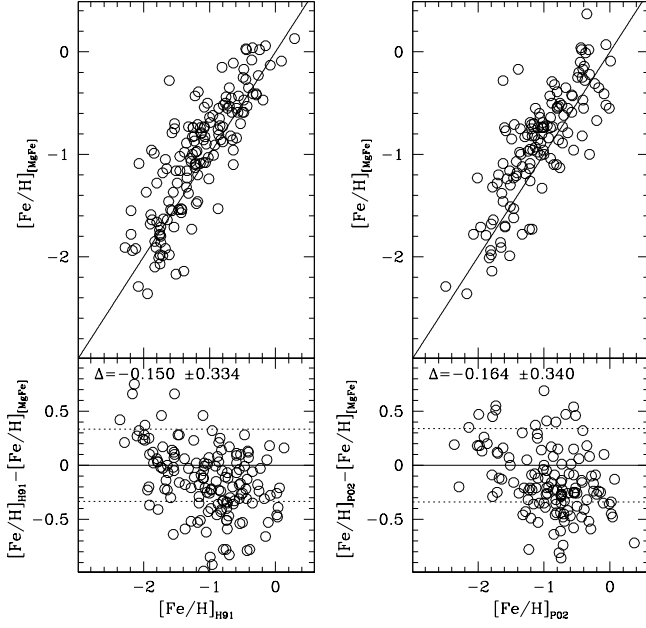


Fig. 10. Comparison of our empirical metallicities of M31 GC with P02 and H91. The solid line indicates the one-to-one relation. The dotted lines in the lower panel enclose the rms. Error bars have been omitted in the panels for clarity.

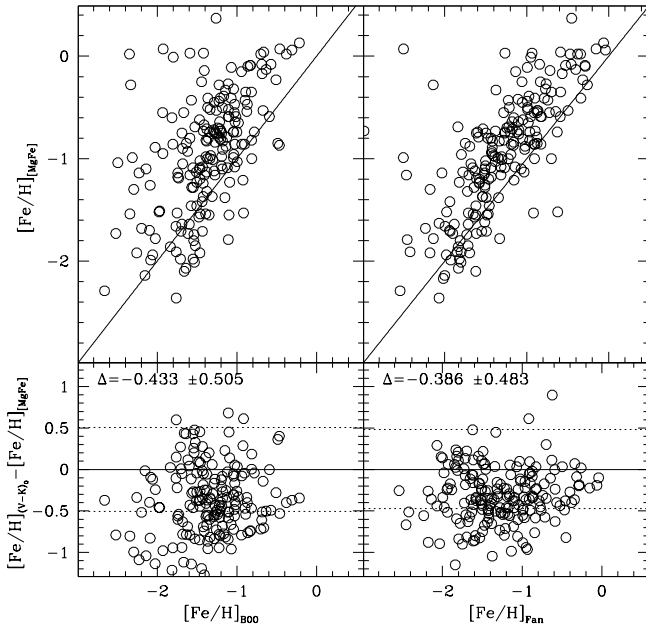


Fig. 11. Comparison of our empirical metallicities of M31 GC with those obtained from $(V - K)_0$ colors, using the calibrations by Barmby et al. (2000) and adopting two different sets of reddening estimates: Barmby et al. (2000) and Fan et al. (2008). The solid line indicates the one-to-one relation and the dotted lines in the lower panel enclose the rms .

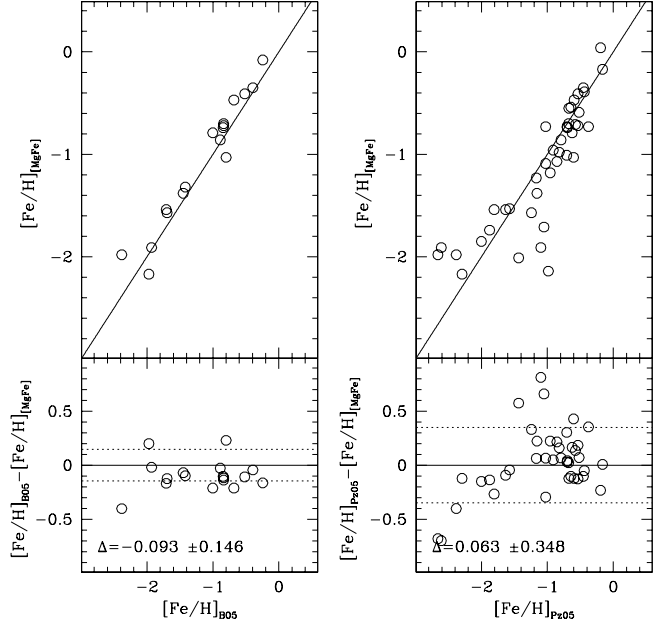


Fig. 12. A comparison of the common GCs between this work, Puzia and Beasley data using $[\text{Fe}/\text{H}]$ definitions by TMB.

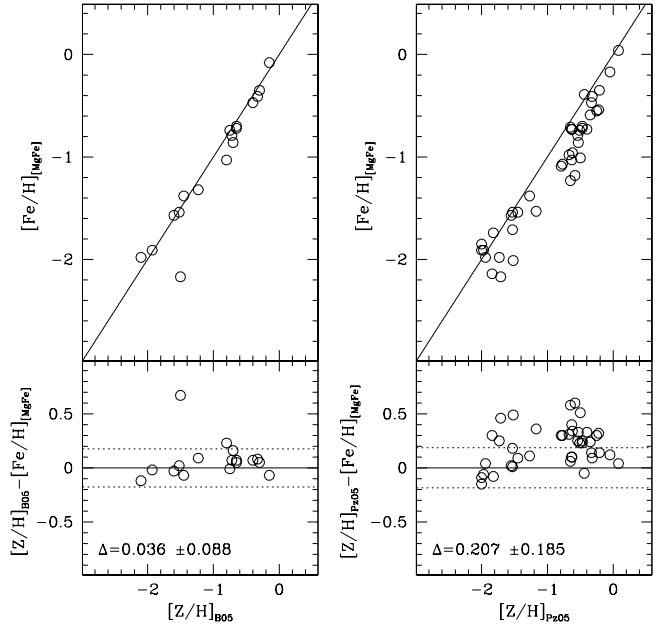


Fig. 13. The same as Fig. 12 but using $[\text{Z}/\text{H}]$.

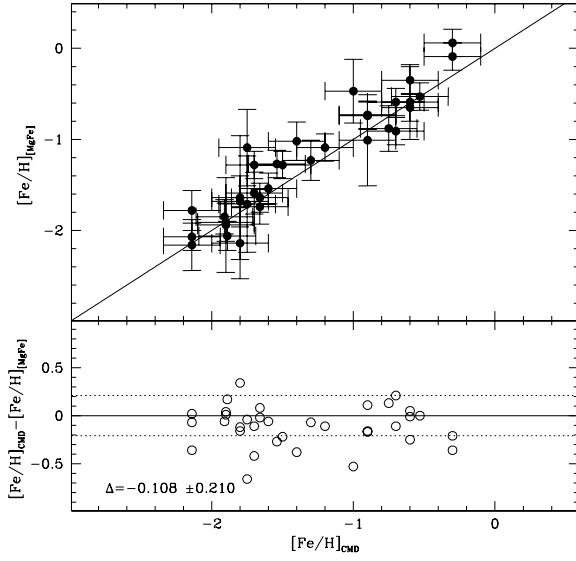


Fig. 14. $[\text{Fe}/\text{H}]$ estimates from CMDs of individual clusters (from good quality HST photometry) are compared with the metallicities derived in the present analysis. The mean offset \pm the standard deviation are reported in the lower panel.

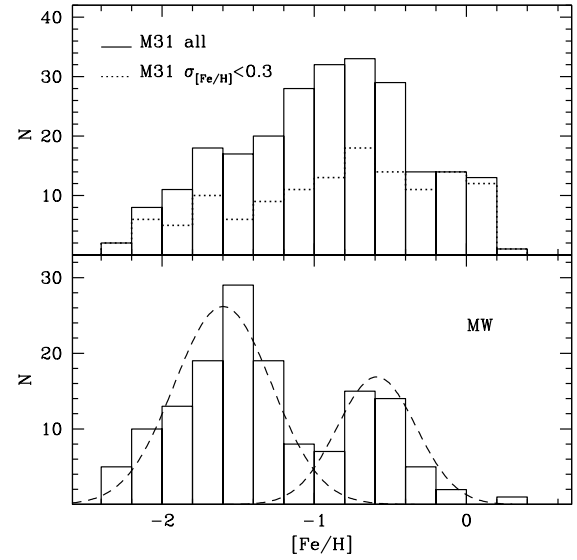


Fig. 15. Metallicity histogram for the M31 globular cluster system (top) and the MW GC system (bottom), reported for comparison. The dashed lines in the lower plot are the gaussian curves in the best fit models as found by the KMM algorithm for two subpopulations ($[\text{Fe}/\text{H}] = -1.60$ and -0.59).

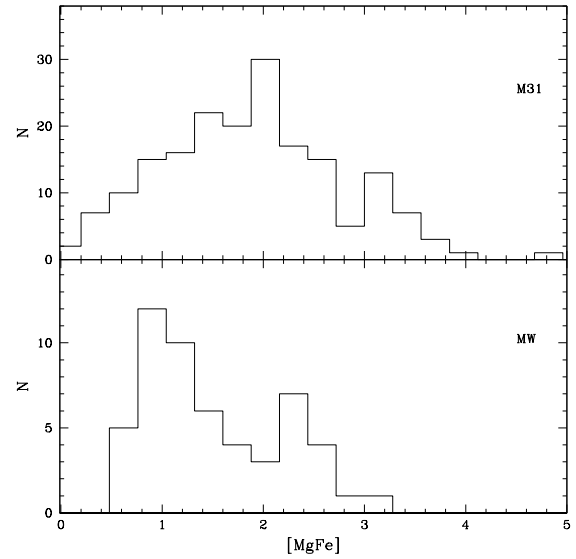


Fig. 16. Distribution of $[\text{MgFe}]$ of the M31 GCs. The lower panel shows the distribution for Milky Way GCs 1 is clearly bimodal.

Table A.1. Lick indices for M31 globular clusters from new observations (Sect. 3.1).

Cluster	Mg ₂ mag	eMg ₂ mag	Mgb Å	eMgb Å	Fe5270 Å	eFe5270 Å	Fe5335 Å	eFe5335 Å	Fe5406 Å	eFe5406 Å	H β Å	eH β Å	y ¹	Set
B003	0.086	0.013	1.554	0.547	1.906	0.648	1.676	0.774	0.643	0.603	2.72	0.39	0	WHT
B006	0.210	0.005	3.051	0.221	2.112	0.262	1.942	0.305	1.389	0.230	1.83	0.17	0	WHT
B012	0.064	0.004	0.619	0.188	0.811	0.223	0.421	0.266	0.303	0.202	2.63	0.13	0	WHT
B017	0.159	0.007	1.979	0.291	1.798	0.338	1.862	0.393	0.957	0.300	1.73	0.22	0	WHT
B019	0.159	0.005	2.313	0.187	1.790	0.222	1.704	0.259	0.916	0.199	1.73	0.14	0	WHT
B020	0.120	0.002	1.962	0.082	1.929	0.092	1.710	0.105	1.406	0.078	1.98	0.07	0	TNG
B022	0.061	0.014	1.339	0.597	1.371	0.712	1.109	0.853	0.209	0.664	3.09	0.42	0	WHT
B023	0.137	0.004	1.929	0.171	1.824	0.186	1.432	0.211	1.205	0.154	1.96	0.17	0	LOI
B032	0.210	0.016	4.270	0.619	2.693	0.730	2.805	0.840	1.221	0.642	1.73	0.53	0	WHT
B034	0.201	0.013	3.339	0.533	2.450	0.631	1.916	0.744	1.656	0.555	1.15	0.41	0	WHT
B039	0.176	0.008	2.630	0.320	1.920	0.370	1.742	0.429	0.880	0.326	1.40	0.26	0	WHT
B042	0.161	0.008	2.204	0.325	1.629	0.374	1.458	0.432	0.997	0.323	1.87	0.27	0	WHT
B051	0.170	0.010	2.565	0.397	1.608	0.467	1.054	0.553	0.746	0.416	1.37	0.31	0	WHT
B058	0.097	0.007	1.452	0.294	1.220	0.352	1.478	0.402	0.812	0.312	2.34	0.24	0	LOI
B060	0.134	0.012	2.067	0.518	1.474	0.622	0.691	0.744	0.916	0.560	2.53	0.37	5	WHT
B070	0.123	0.010	1.358	0.406	0.976	0.481	0.944	0.564	0.292	0.436	2.53	0.29	5	WHT
B071	0.275	0.013	4.838	0.499	2.710	0.598	2.279	0.702	1.725	0.532	2.04	0.38	0	WHT
B073	0.207	0.012	3.623	0.465	2.767	0.546	2.572	0.635	1.235	0.490	2.21	0.35	0	WHT
B082	0.193	0.012	2.608	0.467	2.111	0.526	1.955	0.604	0.835	0.459	1.63	0.40	0	WHT
B083	0.037	0.011	0.787	0.442	0.977	0.494	0.677	0.575	0.826	0.423	1.72	0.42	2	WHT
B095	0.186	0.017	2.754	0.710	1.149	0.846	1.592	0.973	2.058	0.700	1.59	0.55	0	WHT
B099	0.166	0.010	2.216	0.412	1.680	0.485	1.374	0.571	0.824	0.437	1.74	0.30	0	WHT
B110	0.183	0.009	2.655	0.359	1.738	0.424	1.788	0.491	1.302	0.370	1.64	0.28	0	WHT
B111	0.144	0.019	2.342	0.774	1.845	0.923	1.084	1.079	0.804	0.819	1.60	0.60	0	WHT
B117	0.067	0.005	0.897	0.206	0.630	0.232	0.621	0.265	0.253	0.196	2.06	0.20	4	WHT
B131	0.279	0.005	4.067	0.204	2.389	0.243	2.118	0.285	1.485	0.218	1.57	0.15	0	WHT
B147	0.242	0.002	3.952	0.082	3.032	0.091	2.816	0.103	2.162	0.076	1.66	0.08	0	TNG
B148	0.240	0.008	4.036	0.299	2.946	0.326	2.743	0.368	0.911	0.283	3.74	0.28	0	WHT
B151	0.199	0.006	3.179	0.227	1.981	0.269	1.879	0.312	1.347	0.235	1.75	0.18	0	WHT
B153	0.247	0.011	4.057	0.432	2.427	0.513	2.228	0.598	1.860	0.450	1.55	0.34	0	WHT
B155	0.212	0.010	2.732	0.405	3.711	0.420	3.685	0.469	1.221	0.364	3.24	0.38	0	WHT
B156	0.078	0.009	1.259	0.376	1.400	0.410	1.224	0.465	0.571	0.345	1.99	0.38	0	WHT
B158	0.149	0.012	1.744	0.499	2.278	0.570	1.982	0.670	1.575	0.507	1.01	0.38	0	WHT
B162	0.270	0.015	4.720	0.602	2.198	0.738	2.727	0.843	1.623	0.646	1.91	0.46	0	WHT
B163	0.235	0.005	4.301	0.187	2.797	0.206	2.466	0.231	1.555	0.170	1.59	0.20	0	WHT
B169	0.280	0.013	5.389	0.486	2.657	0.543	1.977	0.624	2.404	0.447	1.65	0.52	0	WHT
B171	0.214	0.002	3.610	0.091	2.663	0.102	2.245	0.116	1.979	0.085	1.89	0.09	0	TNG
B174	0.103	0.006	1.950	0.243	1.417	0.270	1.194	0.306	0.892	0.225	1.89	0.25	0	WHT
B178	0.079	0.006	1.354	0.226	1.191	0.249	1.639	0.280	0.420	0.209	2.98	0.23	0	WHT
B179	0.116	0.008	1.933	0.317	1.408	0.350	1.520	0.396	0.648	0.299	1.10	0.32	0	WHT
B180	0.125	0.006	2.589	0.216	1.924	0.244	1.146	0.283	0.603	0.215	1.57	0.21	0	WHT
B182	0.146	0.014	2.776	0.554	1.593	0.667	0.878	0.799	0.328	0.607	1.92	0.42	0	WHT
B183	0.182	0.006	3.134	0.221	2.361	0.244	1.423	0.283	0.922	0.211	1.92	0.22	0	WHT
B185	0.159	0.007	2.834	0.289	2.258	0.316	1.745	0.358	0.893	0.261	1.70	0.31	0	WHT
B187	0.123	0.012	1.370	0.494	0.892	0.547	0.653	0.624	0.447	0.461	2.52	0.45	0	WHT
B193	0.233	0.004	4.182	0.167	3.071	0.183	2.631	0.207	1.558	0.155	1.92	0.17	0	WHT
B204	0.139	0.005	2.642	0.204	2.256	0.223	2.733	0.249	1.415	0.185	1.94	0.21	0	WHT
B206	0.082	0.004	1.494	0.143	1.516	0.157	1.293	0.179	0.837	0.131	2.23	0.14	0	WHT
B212	0.050	0.005	1.009	0.219	0.183	0.252	0.245	0.288	0.358	0.212	2.43	0.21	0	WHT
B215	0.196	0.007	3.493	0.288	2.306	0.320	1.758	0.364	0.861	0.273	1.92	0.29	0	WHT
B218	0.130	0.002	2.137	0.065	1.923	0.073	1.598	0.083	1.331	0.062	2.05	0.06	0	TNG
B219	0.157	0.009	3.211	0.339	2.070	0.386	1.241	0.449	1.057	0.344	2.41	0.32	0	WHT
B224	0.042	0.006	0.909	0.263	0.448	0.299	1.162	0.339	0.177	0.258	2.17	0.24	0	WHT
B225	0.170	0.002	3.279	0.077	2.464	0.085	2.167	0.098	1.021	0.074	1.77	0.08	0	WHT
B228	0.129	0.007	2.104	0.300	1.759	0.328	1.473	0.375	1.594	0.272	2.19	0.29	0	WHT
B230	0.057	0.007	0.107	0.286	0.461	0.315	0.174	0.363	0.267	0.268	2.53	0.26	0	WHT
B232	0.032	0.005	0.493	0.214	0.404	0.236	0.690	0.267	0.236	0.197	2.38	0.21	4	WHT
B233	0.099	0.005	1.709	0.192	1.883	0.210	1.629	0.240	0.825	0.181	2.04	0.18	0	WHT
B235	0.133	0.006	2.380	0.222	1.690	0.246	1.773	0.279	0.973	0.207	1.96	0.22	0	WHT
B236	0.052	0.012	0.767	0.486	0.318	0.534	0.009	0.613	0.320	0.441	4.40	0.46	0	WHT
B238	0.137	0.006	3.478	0.231	1.714	0.267	1.862	0.301	0.873	0.225	1.78	0.24	0	WHT
B240	0.044	0.005	1.060	0.185	1.252	0.206	0.677	0.239	0.212	0.179	2.38	0.18	0	WHT
B318	0.027	0.004	0.112	0.165	0.586	0.190	0.231	0.222	0.601	0.165	5.49	0.12	1	TNG
B338	0.082	0.002	1.250	0.078	1.454	0.088	1.223	0.102	1.194	0.075	2.24	0.07	0	TNG
B344	0.109	0.007	1.669	0.270	2.161	0.291	2.320	0.330	1.114	0.249	1.85	0.26	0	WHT

Table A.1. continued.

Cluster	Mg ₂ mag	eMg ₂ mag	Mgb Å	eMgb Å	Fe5270 Å	eFe5270 Å	Fe5335 Å	eFe5335 Å	Fe5406 Å	eFe5406 Å	H β Å	eH β Å	y ¹	Set
B347	0.052	0.007	1.175	0.274	0.447	0.311	0.994	0.351	0.179	0.265	2.46	0.26	4	WHT
B348	0.136	0.008	2.169	0.303	2.221	0.327	1.443	0.383	1.061	0.284	2.52	0.28	0	WHT
B356	0.075	0.008	0.877	0.325	1.133	0.353	0.817	0.405	0.378	0.297	2.44	0.31	0	WHT
B358	0.023	0.003	0.230	0.122	0.599	0.137	0.296	0.159	0.649	0.116	2.91	0.11	0	TNG
B373	0.167	0.016	2.451	0.619	2.169	0.832	1.940	0.810	1.435	0.611	1.55	0.53	0	WHT
B381	0.075	0.006	1.372	0.257	1.766	0.283	1.650	0.323	0.722	0.242	1.67	0.25	0	WHT
B399	0.043	0.004	0.817	0.178	0.854	0.201	1.164	0.229	0.752	0.170	2.89	0.16	0	TNG
B457	0.265	0.000	4.029	0.013	3.851	0.014	3.496	0.016	2.891	0.012	1.44	0.01	0	TNG
B468	0.113	0.007	2.583	0.277	1.472	0.320	1.095	0.367	0.657	0.274	2.50	0.25	4	TNG
B472	0.080	0.004	3.214	0.142	1.378	0.168	1.266	0.192	0.514	0.143	2.23	0.15	0	WHT
G001	0.133	0.003	2.187	0.104	1.866	0.115	1.915	0.131	0.936	0.098	2.37	0.10	0	LOI
B020D	0.092	0.016	1.713	0.653	0.340	0.805	0.897	0.917	0.602	0.696	3.22	0.49	0	WHT
VDB0	0.031	0.002	0.186	0.088	0.598	0.101	0.568	0.116	0.366	0.087	4.50	0.07	1	TNG
B025D*	0.250	0.024	4.182	0.955	1.875	1.094	2.463	1.258	0.035	1.008	0.08	0.86	0	WHT
B041D	0.126	0.020	0.685	0.851	1.416	0.945	1.897	1.075	1.019	0.817	1.97	0.65	0	WHT
B046D*	0.230	0.026	3.245	1.091	2.712	1.255	3.013	1.454	1.154	1.160	2.12	0.76	0	WHT
B090D	0.291	0.007	4.122	0.298	2.604	0.349	2.241	0.408	1.732	0.310	1.51	0.23	0	WHT
B215D*	0.187	0.009	2.449	0.392	1.676	0.463	1.450	0.547	1.061	0.414	1.79	0.28	0	WHT
B344D	0.121	0.001	2.517	0.022	2.054	0.024	1.679	0.028	1.372	0.021	2.66	0.02	0	TNG
B514	0.062	0.003	0.300	0.137	0.176	0.154	1.279	0.169	0.282	0.159	2.32	0.13	0	LOI
MCGC1	0.041	0.007	0.566	0.290	0.489	0.327	0.005	0.379	0.397	0.276	1.84	0.29	0	LOI
MCGC8	0.093	0.003	1.334	0.115	1.400	0.128	1.206	0.147	1.041	0.109	1.98	0.10	0	TNG
MCGC10	0.031	0.003	0.395	0.104	0.633	0.118	0.427	0.136	0.677	0.100	2.93	0.09	0	TNG

¹ y=BLCC (young cluster) from Fusi Pecci et al. (2005) 0– old cluster; 1– color selected; 2– H_{β} selected; 3– color and H_{β} selected; 4– reportedly young objects by other authors and candidates BLCC (table 2)

* B025D, B046D and B215D are classified by Caldwell et al. (2009) to be not-clusters and in the following analysis are not considered.

Table A.2. Lick indices M31 globular clusters taken from literature sources and reported into the T98 system (Sect. 3.2).

Cluster	Mg ₂ mag	eMg ₂ mag	Mgb Å	eMgb Å	Fe5270 Å	eFe5270 Å	Fe5335 Å	eFe5335 Å	Fe5406 Å	eFe5406 Å	H β Å	eH β Å	y ¹	Set ²
B001	0.160	0.033	2.485	0.631	2.366	0.422	2.753	0.485	99.999	99.999	2.17	0.30	0	4
B003	0.086	0.013	1.554	0.547	1.906	0.648	1.676	0.774	0.643	0.603	2.75	0.39	0	3
B004	0.081	0.033	2.094	0.631	0.772	0.422	1.846	0.485	99.999	99.999	3.16	0.30	0	4
B005	0.153	0.033	2.379	0.631	2.033	0.422	1.021	0.485	99.999	99.999	2.05	0.30	0	4
B006	0.144	0.016	2.449	0.620	2.060	0.630	2.010	0.630	1.163	0.630	2.00	0.56	0	1
B008	0.144	0.033	2.005	0.631	2.893	0.422	2.984	0.485	99.999	99.999	3.67	0.30	2	4
B009	0.060	0.021	1.246	0.035	1.160	0.031	99.999	99.999	99.999	99.999	3.31	0.03	0	5
B010	0.073	0.033	0.628	0.631	1.561	0.422	1.021	0.485	99.999	99.999	3.00	0.30	0	4
B011	0.046	0.021	1.081	0.035	1.649	0.032	99.999	99.999	99.999	99.999	1.79	0.04	0	5
B012	0.064	0.004	0.619	0.188	0.811	0.223	0.421	0.266	0.303	0.202	2.66	0.13	0	3
B013	0.185	0.033	1.085	0.631	4.366	0.422	3.050	0.485	99.999	99.999	2.89	0.30	0	4
B015	0.362	0.010	6.430	0.292	4.160	0.275	3.300	0.317	1.990	0.237	1.53	0.27	4	0
B016	0.130	0.033	2.952	0.631	1.899	0.422	1.778	0.485	99.999	99.999	1.72	0.30	0	4
B017	0.159	0.007	1.979	0.291	1.798	0.338	1.862	0.393	0.957	0.300	1.76	0.22	0	3
B018	0.090	0.033	1.733	0.631	1.999	0.422	2.453	0.485	99.999	99.999	2.40	0.30	7	4
B019	0.159	0.005	2.313	0.187	1.790	0.222	1.704	0.259	0.916	0.199	1.76	0.14	0	3
B020	0.120	0.002	1.962	0.082	1.929	0.092	1.710	0.105	1.406	0.078	1.98	0.07	0	6
B021	0.109	0.033	2.659	0.631	1.254	0.422	1.778	0.485	99.999	99.999	1.91	0.30	0	4
B022	0.061	0.014	1.339	0.597	1.371	0.712	1.109	0.853	0.209	0.664	3.12	0.42	0	3
B023	0.137	0.004	1.929	0.171	1.824	0.186	1.432	0.211	1.205	0.154	1.96	0.17	0	7
B024	0.163	0.019	2.741	0.032	1.997	0.028	99.999	99.999	99.999	99.999	1.22	0.03	0	5
B025	0.088	0.019	0.997	0.870	1.480	0.880	0.610	0.880	0.253	0.880	3.24	0.78	0	1
B026	0.213	0.033	4.461	0.631	1.832	0.422	2.620	0.485	99.999	99.999	1.48	0.30	0	4
B027	0.052	0.014	0.860	0.022	0.776	0.020	99.999	99.999	99.999	99.999	2.39	0.02	0	5
B028	0.092	0.033	1.347	0.631	1.764	0.422	-0.395	0.485	99.999	99.999	3.98	0.30	2	4
B029	0.171	0.033	3.607	0.631	3.988	0.422	2.486	0.485	99.999	99.999	0.50	0.30	0	4
B030	0.228	0.033	2.694	0.631	3.797	0.422	3.083	0.485	99.999	99.999	1.79	0.30	4	4
B031	0.111	0.033	2.572	0.631	-0.346	0.422	0.847	0.485	99.999	99.999	0.80	0.30	0	4
B032	0.210	0.016	4.270	0.619	2.693	0.730	2.805	0.840	1.221	0.642	1.76	0.53	0	3
B033	0.079	0.033	1.217	0.631	1.798	0.422	1.948	0.485	99.999	99.999	3.30	0.30	0	4
B034	0.122	0.011	1.830	0.490	1.490	0.500	1.680	0.500	0.863	0.500	2.18	0.47	0	1
B035	0.080	0.033	1.825	0.631	1.254	0.422	3.669	0.485	99.999	99.999	2.45	0.30	0	4
B037	0.100	0.033	1.825	0.631	3.477	0.422	1.914	0.485	99.999	99.999	99.99	9.99	0	4
B038	0.090	0.033	0.782	0.631	1.289	0.422	-0.143	0.485	99.999	99.999	2.89	0.30	0	4
B039	0.176	0.008	2.630	0.320	1.920	0.370	1.742	0.429	0.880	0.326	1.43	0.26	0	3
B040	0.019	0.033	0.743	0.631	-0.321	0.422	1.982	0.485	99.999	99.999	7.58	0.30	3	4
B041	0.047	0.033	1.217	0.631	1.595	0.422	1.982	0.485	99.999	99.999	2.73	0.30	0	4
B042	0.161	0.008	2.204	0.325	1.629	0.374	1.458	0.432	0.997	0.323	1.90	0.27	0	3
B043	0.040	0.033	0.512	0.631	0.807	0.422	0.567	0.485	99.999	99.999	5.70	0.30	3	4
B044	0.105	0.031	4.037	0.049	2.148	0.046	99.999	99.999	99.999	99.999	99.99	9.99	0	5
B045	0.138	0.014	1.417	0.640	2.290	0.640	1.530	0.640	1.323	0.650	2.34	0.56	0	1
B046	0.115	0.039	-0.126	0.065	1.071	0.061	99.999	99.999	99.999	99.999	1.98	0.06	0	5
B047	0.207	0.036	2.427	0.061	-2.290	0.056	99.999	99.999	99.999	99.999	2.69	0.06	2	5
B048	0.151	0.019	2.219	0.860	2.370	0.860	2.380	0.880	0.493	0.880	2.90	0.77	0	1
B049	0.052	0.033	1.272	0.631	1.629	0.422	-0.793	0.485	99.999	99.999	9.48	0.30	3	4
B050	0.089	0.033	1.951	0.631	0.144	0.422	1.846	0.485	99.999	99.999	1.86	0.30	0	4
B051	0.170	0.016	1.983	0.730	2.530	0.740	1.630	0.740	1.393	0.740	1.80	0.67	0	1
B054	0.207	0.033	3.391	0.631	3.024	0.422	2.786	0.485	99.999	99.999	1.77	0.30	0	4
B055	0.161	0.033	3.408	0.631	1.561	0.422	2.719	0.485	99.999	99.999	2.80	0.30	0	4
B056	0.229	0.033	3.755	0.631	3.829	0.422	2.819	0.485	99.999	99.999	1.77	0.30	0	4
B057	0.076	0.033	1.291	0.631	2.795	0.422	-0.539	0.485	99.999	99.999	5.73	0.30	2	4
B058	0.070	0.009	1.860	0.270	1.900	0.254	0.980	0.275	0.910	0.220	2.16	0.25	0	0
B059	0.144	0.033	3.391	0.631	1.865	0.422	0.496	0.485	99.999	99.999	1.21	0.30	0	4
B060	0.134	0.012	2.067	0.518	1.474	0.622	0.691	0.744	0.916	0.560	2.56	0.37	1	3
B061	0.187	0.033	2.728	0.631	2.598	0.422	1.436	0.485	99.999	99.999	3.12	0.30	0	4
B063	0.141	0.020	1.735	0.032	1.317	0.029	99.999	99.999	99.999	99.999	1.20	0.03	0	5
B064	0.077	0.020	0.357	0.033	1.802	0.030	99.999	99.999	99.999	99.999	1.77	0.03	0	5
B065	0.080	0.033	1.402	0.631	1.663	0.422	0.952	0.485	99.999	99.999	2.22	0.30	0	4
B066	0.055	0.033	0.991	0.631	0.319	0.422	-0.467	0.485	99.999	99.999	4.84	0.30	3	4
B068	0.187	0.024	4.062	0.041	1.428	0.034	99.999	99.999	99.999	99.999	0.49	0.04	0	5
B069	0.135	0.033	1.384	0.631	1.730	0.422	2.386	0.485	99.999	99.999	7.34	0.30	3	4
B070	0.123	0.010	1.358	0.406	0.976	0.481	0.944	0.564	0.292	0.436	2.56	0.29	1	3
B071	0.275	0.013	4.838	0.499	2.710	0.598	2.279	0.702	1.725	0.532	2.06	0.38	0	3
B072	0.164	0.033	2.641	0.631	3.284	0.422	2.520	0.485	99.999	99.999	2.15	0.30	0	4
B073	0.207	0.012	3.623	0.465	2.767	0.546	2.572	0.635	1.235	0.490	2.24	0.35	0	3

Table A.2. continued.

Cluster	Mg ₂ mag	eMg ₂ mag	Mgb Å	eMgb Å	Fe5270 Å	eFe5270 Å	Fe5335 Å	eFe5335 Å	Fe5406 Å	eFe5406 Å	H β Å	eH β Å	y ¹	Set ²
B074	0.078	0.033	0.609	0.631	1.152	0.422	0.426	0.485	99.999	99.999	4.09	0.30	2	4
B075	0.048	0.033	1.697	0.631	-0.784	0.422	2.620	0.485	99.999	99.999	2.17	0.30	0	4
B076	0.133	0.033	2.641	0.631	0.249	0.422	2.218	0.485	99.999	99.999	3.21	0.30	0	4
B081	0.036	0.033	0.648	0.631	0.945	0.422	1.778	0.485	99.999	99.999	8.15	0.30	3	4
B082	0.193	0.012	2.608	0.467	2.111	0.526	1.955	0.604	0.835	0.459	1.66	0.40	0	3
B083	0.037	0.011	0.787	0.442	0.977	0.494	0.677	0.575	0.826	0.423	1.75	0.42	2	3
B085	0.014	0.021	0.916	0.034	1.160	0.031	99.999	99.999	99.999	99.999	3.31	0.03	0	5
B086	0.038	0.015	-0.443	0.025	1.183	0.022	99.999	99.999	99.999	99.999	2.55	0.03	0	5
B088	0.043	0.033	0.820	0.631	0.108	0.422	0.742	0.485	99.999	99.999	2.77	0.30	0	4
B090	0.218	0.033	3.308	0.631	3.381	0.422	1.982	0.485	99.999	99.999	3.45	0.30	4	4
B091	0.116	0.033	1.384	0.631	1.932	0.422	1.880	0.485	99.999	99.999	7.47	0.30	3	4
B092	0.100	0.024	1.843	0.039	0.410	0.035	99.999	99.999	99.999	99.999	1.79	0.04	0	5
B093	0.123	0.033	1.933	0.631	2.167	0.422	2.016	0.485	99.999	99.999	3.14	0.30	0	4
B094	0.131	0.033	2.797	0.631	2.598	0.422	2.386	0.485	99.999	99.999	2.31	0.30	0	4
B095	0.186	0.017	2.754	0.710	1.149	0.846	1.592	0.973	2.058	0.700	1.62	0.55	0	3
B096	0.215	0.031	2.974	0.055	3.055	0.042	99.999	99.999	99.999	99.999	1.44	0.05	0	5
B097	0.124	0.033	1.569	0.631	2.400	0.422	1.402	0.485	99.999	99.999	2.87	0.30	0	4
B098	0.182	0.027	4.602	0.045	1.649	0.040	99.999	99.999	99.999	99.999	1.53	0.04	0	5
B099	0.166	0.010	2.216	0.412	1.680	0.485	1.374	0.571	0.824	0.437	1.77	0.30	0	3
B103	0.184	0.013	3.333	0.021	1.250	0.018	99.999	99.999	99.999	99.999	1.56	0.02	0	5
B105	0.120	0.033	1.513	0.631	2.033	0.422	2.016	0.485	99.999	99.999	1.67	0.30	0	4
B106	0.135	0.033	0.943	0.056	1.932	0.050	99.999	99.999	99.999	99.999	0.67	0.05	0	5
B107	0.093	0.014	1.219	0.023	1.824	0.020	99.999	99.999	99.999	99.999	2.02	0.02	0	5
B109	0.250	0.033	2.711	0.631	2.828	0.422	2.719	0.485	99.999	99.999	99.99	9.99	0	4
B110	0.183	0.009	2.655	0.359	1.738	0.424	1.788	0.491	1.302	0.370	1.67	0.28	0	3
B111	0.144	0.019	2.342	0.774	1.845	0.923	1.084	1.079	0.804	0.819	1.63	0.60	0	3
B112	0.291	0.038	5.997	0.063	3.727	0.054	99.999	99.999	99.999	99.999	2.09	0.06	0	5
B115	0.273	0.013	3.862	0.022	1.976	0.018	99.999	99.999	99.999	99.999	0.12	0.02	0	5
B116	0.171	0.033	2.326	0.631	2.598	0.422	2.252	0.485	99.999	99.999	2.73	0.30	0	4
B117	0.067	0.005	0.897	0.206	0.630	0.232	0.621	0.265	0.253	0.196	2.09	0.20	4	3
B119	0.226	0.033	3.524	0.631	2.532	0.422	1.982	0.485	99.999	99.999	1.65	0.30	0	4
B122	0.171	0.033	1.679	0.631	2.100	0.422	0.249	0.485	99.999	99.999	2.61	0.30	0	4
B125	0.063	0.033	1.440	0.631	-0.367	0.422	0.777	0.485	99.999	99.999	3.21	0.30	0	4
B126	0.046	0.014	1.280	0.240	1.020	0.170	0.810	0.200	0.470	0.140	3.65	0.14	0	2
B127	0.189	0.004	2.716	0.210	3.020	0.210	0.950	0.210	1.203	0.210	1.68	0.20	0	1
B129	0.183	0.033	2.449	0.631	3.024	0.422	0.532	0.485	99.999	99.999	2.73	0.30	0	4
B130	0.070	0.033	1.458	0.631	0.876	0.422	1.880	0.485	99.999	99.999	3.43	0.30	0	4
B131	0.279	0.005	4.067	0.204	2.389	0.243	2.118	0.285	1.485	0.218	1.60	0.15	0	3
B134	0.109	0.014	2.220	0.240	1.790	0.170	1.590	0.200	0.990	0.150	1.78	0.16	0	2
B135	0.076	0.033	1.160	0.631	1.323	0.422	0.777	0.485	99.999	99.999	2.26	0.30	0	4
B137	0.099	0.033	0.915	0.631	1.999	0.422	1.914	0.485	99.999	99.999	2.84	0.30	0	4
B140	0.247	0.033	3.706	0.631	3.251	0.422	0.812	0.485	99.999	99.999	0.18	0.30	0	4
B141	0.072	0.033	0.686	0.631	0.529	0.422	1.470	0.485	99.999	99.999	2.93	0.30	0	4
B143	0.241	0.015	4.136	0.026	2.256	0.023	99.999	99.999	99.999	99.999	1.53	0.03	0	5
B144	0.187	0.011	2.647	0.470	2.430	0.470	1.570	0.480	1.143	0.480	1.76	0.46	0	1
B146	0.171	0.042	5.672	0.066	3.985	0.059	99.999	99.999	99.999	99.999	0.20	0.07	4	5
B147	0.242	0.002	3.952	0.082	3.032	0.091	2.816	0.103	2.162	0.076	1.66	0.08	0	6
B148	0.145	0.010	2.151	0.390	1.960	0.390	2.040	0.390	1.263	0.390	2.01	0.37	0	1
B149	0.090	0.033	1.328	0.631	2.200	0.422	1.948	0.485	99.999	99.999	2.93	0.30	0	4
B151	0.199	0.006	3.179	0.227	1.981	0.269	1.879	0.312	1.347	0.235	1.78	0.18	0	3
B152	0.062	0.026	2.295	0.042	2.170	0.039	99.999	99.999	99.999	99.999	1.22	0.04	0	5
B153	0.247	0.011	4.057	0.432	2.427	0.513	2.228	0.598	1.860	0.450	1.58	0.34	0	3
B154	0.265	0.029	4.963	0.047	3.034	0.044	99.999	99.999	99.999	99.999	1.65	0.05	4	5
B155	0.212	0.010	2.732	0.405	3.711	0.420	3.685	0.469	1.221	0.364	3.27	0.38	0	3
B156	0.078	0.009	1.259	0.376	1.400	0.410	1.224	0.465	0.571	0.345	2.02	0.38	0	3
B158	0.130	0.013	2.270	0.210	1.860	0.100	1.700	0.130	1.060	0.090	1.74	0.10	0	2
B159	0.177	0.033	2.113	0.631	2.300	0.422	1.367	0.485	99.999	99.999	2.57	0.30	0	4
B161	0.180	0.033	2.237	0.631	2.167	0.422	1.436	0.485	99.999	99.999	1.98	0.30	0	4
B162	0.270	0.015	4.720	0.602	2.198	0.738	2.727	0.843	1.623	0.646	1.94	0.46	0	3
B163	0.222	0.013	4.010	0.190	2.600	0.070	2.440	0.090	1.570	0.060	1.74	0.07	0	2
B164	0.216	0.033	3.308	0.631	1.561	0.422	2.319	0.485	99.999	99.999	1.65	0.30	4	4
B165	0.050	0.025	-0.328	0.041	1.693	0.038	99.999	99.999	99.999	99.999	2.51	0.04	0	5
B167	0.180	0.033	3.037	0.631	3.154	0.422	2.083	0.485	99.999	99.999	2.03	0.30	0	4
B169	0.280	0.013	5.389	0.486	2.657	0.543	1.977	0.624	2.404	0.447	1.68	0.52	0	3
B170	0.116	0.033	3.424	0.631	0.354	0.422	2.050	0.485	99.999	99.999	4.69	0.30	2	4
B171	0.189	0.011	3.110	0.314	2.340	0.296	2.400	0.338	1.550	0.256	2.27	0.29	0	0

Table A.2. continued.

Cluster	Mg ₂ mag	eMg ₂ mag	Mgb Å	eMgb Å	Fe5270 Å	eFe5270 Å	Fe5335 Å	eFe5335 Å	Fe5406 Å	eFe5406 Å	H β Å	eH β Å	y ¹	Set ²
B171	0.214	0.002	3.610	0.091	2.663	0.102	2.245	0.116	1.979	0.085	1.89	0.09	0	6
B174	0.103	0.006	1.950	0.243	1.417	0.270	1.194	0.306	0.892	0.225	1.92	0.25	0	3
B178	0.097	0.009	1.890	0.270	1.930	0.254	0.310	0.229	0.730	0.220	1.97	0.25	0	0
B179	0.116	0.008	1.933	0.317	1.408	0.350	1.520	0.396	0.648	0.299	1.13	0.32	0	3
B180	0.125	0.006	2.589	0.216	1.924	0.244	1.146	0.283	0.603	0.215	1.60	0.21	0	3
B182	0.076	0.011	1.700	0.460	1.740	0.470	1.660	0.470	0.803	0.470	2.39	0.42	0	1
B183	0.182	0.006	3.134	0.221	2.361	0.244	1.423	0.283	0.922	0.211	1.95	0.22	0	3
B184	0.219	0.033	4.398	0.631	2.532	0.422	2.553	0.485	99.999	99.999	1.79	0.30	0	4
B185	0.159	0.007	2.834	0.289	2.258	0.316	1.745	0.358	0.893	0.261	1.73	0.31	0	3
B187	0.123	0.012	1.370	0.494	0.892	0.547	0.653	0.624	0.447	0.461	2.55	0.45	0	3
B188	0.094	0.033	1.624	0.631	0.038	0.422	1.298	0.485	99.999	99.999	2.43	0.30	0	4
B190	0.094	0.033	1.915	0.631	2.066	0.422	1.812	0.485	99.999	99.999	2.52	0.30	0	4
B193	0.233	0.004	4.182	0.167	3.071	0.183	2.631	0.207	1.558	0.155	1.95	0.17	0	3
B197	0.234	0.033	3.998	0.631	2.991	0.422	2.786	0.485	99.999	99.999	1.31	0.30	4	4
B198	0.160	0.033	2.255	0.631	2.532	0.422	2.184	0.485	99.999	99.999	2.33	0.30	0	4
B199	0.068	0.033	0.877	0.631	0.494	0.422	1.091	0.485	99.999	99.999	3.16	0.30	0	4
B200	0.111	0.033	2.728	0.631	1.391	0.422	3.181	0.485	99.999	99.999	2.17	0.30	0	4
B201	0.106	0.017	2.216	0.028	2.019	0.027	99.999	99.999	99.999	99.999	1.88	0.03	0	5
B203	0.175	0.033	2.745	0.631	2.400	0.422	0.987	0.485	99.999	99.999	1.04	0.30	0	4
B204	0.139	0.005	2.642	0.204	2.256	0.223	2.733	0.249	1.415	0.185	1.97	0.21	0	3
B205	0.097	0.008	1.789	0.013	1.272	0.012	99.999	99.999	99.999	99.999	1.58	0.01	0	5
B206	0.082	0.004	1.494	0.143	1.516	0.157	1.293	0.179	0.837	0.131	2.26	0.14	0	3
B207	0.078	0.033	1.422	0.631	1.932	0.422	1.333	0.485	99.999	99.999	3.23	0.30	0	4
B208	0.220	0.033	2.606	0.631	3.638	0.422	1.914	0.485	99.999	99.999	3.21	0.30	0	4
B209	0.090	0.033	2.077	0.631	1.561	0.422	1.160	0.485	99.999	99.999	2.03	0.30	0	4
B210	0.052	0.033	0.782	0.631	1.186	0.422	1.229	0.485	99.999	99.999	7.00	0.30	3	4
B211	0.028	0.024	1.546	0.039	2.617	0.037	99.999	99.999	99.999	99.999	3.05	0.03	0	5
B212	0.050	0.005	1.009	0.219	0.183	0.252	0.245	0.288	0.358	0.212	2.46	0.21	0	3
B213	0.159	0.033	2.397	0.631	2.233	0.422	1.402	0.485	99.999	99.999	1.26	0.30	0	4
B214	0.071	0.033	1.217	0.631	1.932	0.422	2.586	0.485	99.999	99.999	3.41	0.30	4	4
B215	0.196	0.007	3.493	0.288	2.306	0.320	1.758	0.364	0.861	0.273	1.95	0.29	0	3
B217	0.095	0.033	2.184	0.631	1.595	0.422	1.607	0.485	99.999	99.999	1.98	0.30	0	4
B218	0.123	0.009	2.300	0.261	1.990	0.245	1.710	0.276	1.460	0.213	1.86	0.24	0	0
B219	0.157	0.009	3.211	0.339	2.070	0.386	1.241	0.449	1.057	0.344	2.44	0.32	0	3
B220	0.092	0.033	1.752	0.631	1.391	0.422	1.333	0.485	99.999	99.999	2.26	0.30	0	4
B221	0.135	0.033	1.897	0.631	2.532	0.422	1.229	0.485	99.999	99.999	2.08	0.30	0	4
B222	0.101	0.015	1.300	0.390	1.870	0.370	1.170	0.430	0.970	0.310	4.46	0.31	2	2
B224	0.042	0.006	0.909	0.263	0.448	0.299	1.162	0.339	0.177	0.258	2.20	0.24	0	3
B225	0.187	0.013	3.210	0.190	2.310	0.070	2.030	0.090	1.310	0.060	1.83	0.07	0	2
B228	0.129	0.007	2.104	0.300	1.759	0.328	1.473	0.375	1.594	0.272	2.21	0.29	0	3
B230	0.057	0.007	0.107	0.286	0.461	0.315	0.174	0.363	0.267	0.268	2.56	0.26	0	3
B231	0.102	0.033	2.077	0.631	1.629	0.422	1.710	0.485	99.999	99.999	2.59	0.30	0	4
B232	0.032	0.005	0.493	0.214	0.404	0.236	0.690	0.267	0.236	0.197	2.41	0.21	4	3
B233	0.061	0.015	0.554	0.025	1.736	0.022	99.999	99.999	99.999	99.999	2.16	0.03	0	5
B234	0.113	0.014	2.370	0.240	2.030	0.180	1.500	0.210	0.990	0.150	1.72	0.16	0	2
B235	0.133	0.006	2.380	0.222	1.690	0.246	1.773	0.279	0.973	0.207	1.99	0.22	0	3
B236	0.052	0.012	0.767	0.486	0.318	0.534	0.009	0.613	0.320	0.441	4.43	0.46	0	3
B237	0.070	0.033	-0.357	0.631	3.251	0.422	0.952	0.485	99.999	99.999	7.60	0.30	2	4
B238	0.137	0.006	3.478	0.231	1.714	0.267	1.862	0.301	0.873	0.225	1.81	0.24	0	3
B239	0.068	0.026	1.219	0.043	1.183	0.038	99.999	99.999	99.999	99.999	1.67	0.04	0	5
B240	0.051	0.007	0.750	0.204	0.742	0.190	0.954	0.208	0.723	0.168	2.05	0.19	0	0
B272	0.154	0.033	2.130	0.631	2.300	0.422	1.160	0.485	99.999	99.999	2.05	0.30	0	4
B281	0.160	0.033	1.951	0.631	3.956	0.422	0.952	0.485	99.999	99.999	5.73	0.30	2	4
B283	0.191	0.033	3.475	0.631	-0.140	0.422	3.312	0.485	99.999	99.999	99.99	9.99	0	4
B292	0.053	0.016	0.970	0.400	0.950	0.390	1.140	0.450	0.150	0.340	3.14	0.32	4	2
B293	0.057	0.021	0.860	0.033	1.093	0.032	99.999	99.999	99.999	99.999	3.55	0.03	0	5
B295	0.029	0.033	1.328	0.631	0.633	0.422	0.496	0.485	99.999	99.999	4.94	0.30	2	4
B298	0.040	0.019	-0.356	0.031	0.981	0.026	99.999	99.999	99.999	99.999	2.30	0.03	0	5
B301	0.056	0.015	1.700	0.380	1.430	0.370	1.180	0.420	0.330	0.310	2.94	0.33	0	2
B303	0.119	0.033	1.733	0.631	1.561	0.422	-0.071	0.485	99.999	99.999	5.95	0.30	3	4
B304	0.050	0.015	1.230	0.370	1.400	0.360	0.920	0.420	0.850	0.300	2.52	0.30	0	2
B305	0.052	0.033	2.005	0.631	-0.892	0.422	3.475	0.485	99.999	99.999	2.77	0.30	0	4
B306	0.125	0.033	1.587	0.631	2.200	0.422	0.742	0.485	99.999	99.999	2.47	0.30	0	4
B307	0.053	0.033	2.659	0.631	1.798	0.422	3.050	0.485	99.999	99.999	5.93	0.30	2	4
B310	0.035	0.015	0.920	0.360	1.260	0.350	0.840	0.400	0.440	0.290	2.56	0.30	0	2
B311	0.049	0.012	0.798	0.560	1.100	0.560	0.610	0.560	0.403	0.560	2.80	0.52	4	1

Table A.2. continued.

Cluster	Mg ₂ mag	eMg ₂ mag	Mgb Å	eMgb Å	Fe5270 Å	eFe5270 Å	Fe5335 Å	eFe5335 Å	Fe5406 Å	eFe5406 Å	H β Å	eH β Å	y ¹	Set ²
B312	0.118	0.010	1.448	0.450	2.150	0.450	0.690	0.450	0.443	0.450	2.94	0.43	0	1
B313	0.120	0.014	2.170	0.280	1.690	0.230	1.450	0.260	0.970	0.190	1.51	0.21	0	2
B315	0.089	0.011	0.676	0.470	1.930	0.480	0.110	0.500	0.993	0.510	4.75	0.40	3	1
B316	0.151	0.033	2.237	0.631	2.433	0.422	0.917	0.485	99.999	99.999	2.64	0.30	7	4
B317	0.028	0.030	-0.241	0.048	1.539	0.046	99.999	99.999	99.999	99.999	1.67	0.05	0	5
B318	0.027	0.004	0.112	0.165	0.586	0.190	0.231	0.222	0.601	0.165	5.49	0.12	1	6
B319	0.066	0.033	0.877	0.631	0.668	0.422	0.602	0.485	99.999	99.999	5.54	0.30	2	4
B321	0.032	0.016	0.940	0.430	0.800	0.450	0.730	0.520	0.200	0.380	6.85	0.32	3	2
B322	0.028	0.015	0.350	0.340	0.630	0.330	0.670	0.380	0.450	0.280	5.06	0.24	1	2
B324	0.065	0.014	1.570	0.240	1.660	0.190	1.460	0.220	0.710	0.160	4.69	0.14	4	2
B327	0.057	0.014	0.590	0.250	0.830	0.190	1.100	0.220	0.720	0.160	3.78	0.14	3	2
B328	0.048	0.016	0.190	0.420	0.890	0.410	0.490	0.480	0.400	0.350	2.58	0.35	4	2
B335	0.140	0.033	2.624	0.631	1.186	0.422	1.298	0.485	99.999	99.999	2.31	0.30	0	4
B337	0.064	0.013	1.860	0.190	1.480	0.070	1.110	0.090	0.640	0.060	3.23	0.07	0	2
B338	0.085	0.009	1.220	0.260	1.640	0.245	1.450	0.273	0.730	0.213	2.10	0.24	0	0
B341	0.123	0.033	2.041	0.631	1.254	0.422	1.607	0.485	99.999	99.999	2.05	0.30	0	4
B343	0.086	0.015	1.573	0.024	1.824	0.022	99.999	99.999	99.999	99.999	1.48	0.02	0	5
B344	0.109	0.007	1.669	0.270	2.161	0.291	2.320	0.330	1.114	0.249	1.88	0.26	0	3
B347	0.024	0.014	0.760	0.260	0.510	0.210	0.490	0.240	0.370	0.170	2.87	0.17	4	2
B348	0.136	0.008	2.169	0.303	2.221	0.327	1.443	0.383	1.061	0.284	2.55	0.28	0	3
B350	0.055	0.015	1.130	0.340	0.980	0.320	0.810	0.370	0.330	0.270	2.80	0.27	0	2
B352	0.119	0.026	2.558	0.044	0.201	0.039	99.999	99.999	99.999	99.999	2.82	0.04	0	5
B356	0.075	0.008	0.877	0.325	1.133	0.353	0.817	0.405	0.378	0.297	2.47	0.31	0	3
B357	0.127	0.022	1.191	0.036	1.780	0.033	99.999	99.999	99.999	99.999	2.12	0.03	0	5
B358	0.034	0.007	0.767	0.207	0.810	0.194	0.397	0.187	0.291	0.171	2.63	0.20	1	0
B365	0.060	0.014	1.370	0.260	1.330	0.200	1.000	0.240	0.500	0.180	2.72	0.17	0	2
B366	0.015	0.033	0.763	0.631	-0.339	0.422	0.742	0.485	99.999	99.999	3.07	0.30	0	4
B367	0.050	0.033	0.260	0.631	2.466	0.422	1.021	0.485	99.999	99.999	6.38	0.30	3	4
B370	0.050	0.015	0.913	0.730	-0.080	0.730	0.730	0.740	0.543	0.740	2.71	0.71	0	1
B372	0.117	0.016	1.379	0.660	1.930	0.670	1.610	0.670	0.723	0.670	2.36	0.63	0	1
B373	0.167	0.016	2.451	0.619	2.169	0.832	1.940	0.810	1.435	0.611	1.58	0.53	0	3
B374	0.094	0.033	1.402	0.631	1.932	0.422	1.744	0.485	99.999	99.999	4.24	0.30	3	4
B375	0.128	0.025	0.888	0.044	1.539	0.037	99.999	99.999	99.999	99.999	2.35	0.04	0	5
B376	0.074	0.038	2.348	0.062	0.799	0.060	99.999	99.999	99.999	99.999	6.40	0.06	1	5
B377	0.060	0.030	-1.503	0.051	1.160	0.047	99.999	99.999	99.999	99.999	2.07	0.05	0	5
B378	0.068	0.033	0.972	0.631	1.357	0.422	1.539	0.485	99.999	99.999	3.09	0.30	0	4
B379	0.171	0.020	1.654	0.033	1.516	0.026	99.999	99.999	99.999	99.999	1.48	0.03	0	5
B381	0.075	0.006	1.372	0.257	1.766	0.283	1.650	0.323	0.722	0.242	1.70	0.25	0	3
B382	0.046	0.033	1.532	0.631	1.152	0.422	1.607	0.485	99.999	99.999	3.09	0.30	0	4
B383	0.163	0.013	3.030	0.220	2.120	0.140	1.790	0.170	1.210	0.120	1.75	0.13	0	2
B384	0.163	0.014	1.681	0.024	2.084	0.020	99.999	99.999	99.999	99.999	1.20	0.02	0	5
B386	0.105	0.013	1.410	0.021	2.019	0.019	99.999	99.999	99.999	99.999	2.07	0.02	0	5
B387	0.077	0.020	0.749	0.033	0.686	0.030	99.999	99.999	99.999	99.999	3.44	0.03	0	5
B391	0.077	0.033	1.179	0.631	1.323	0.422	3.637	0.485	99.999	99.999	2.75	0.30	0	4
B393	0.102	0.014	1.490	0.320	1.930	0.280	1.580	0.330	0.700	0.240	1.90	0.24	0	2
B397	0.125	0.025	1.519	0.042	0.868	0.037	99.999	99.999	99.999	99.999	2.30	0.04	0	5
B398	0.162	0.014	3.170	0.300	2.310	0.270	1.710	0.310	1.070	0.230	1.60	0.24	0	2
B399	0.043	0.004	0.817	0.178	0.854	0.201	1.164	0.229	0.752	0.170	2.89	0.16	0	6
B400	0.103	0.033	1.197	0.631	3.348	0.422	-0.215	0.485	99.999	99.999	0.65	0.30	0	4
B401	0.027	0.014	0.530	0.270	0.630	0.230	0.530	0.270	-0.030	0.200	2.84	0.19	0	2
B403	0.208	0.057	3.637	0.097	3.985	0.073	99.999	99.999	99.999	99.999	99.99	9.99	0	5
B405	0.086	0.009	1.274	0.015	0.663	0.021	99.999	99.999	99.999	99.999	2.14	0.01	0	5
B407	0.155	0.017	2.427	0.028	1.317	0.025	99.999	99.999	99.999	99.999	0.59	0.03	0	5
B431	0.066	0.030	-1.234	0.052	1.714	0.044	99.999	99.999	99.999	99.999	1.74	0.04	1	5
B448	0.087	0.033	0.915	0.631	1.083	0.422	-0.503	0.485	99.999	99.999	6.87	0.30	2	4
B457	0.265	0.000	4.029	0.013	3.851	0.014	3.496	0.016	2.891	0.012	1.44	0.01	0	6
B458	0.102	0.033	0.820	0.631	2.333	0.422	2.419	0.485	99.999	99.999	6.36	0.30	3	4
B467	0.074	0.033	0.338	0.631	-0.033	0.422	0.391	0.485	99.999	99.999	2.33	0.30	0	4
B468	0.113	0.007	2.583	0.277	1.472	0.320	1.095	0.367	0.657	0.274	2.50	0.25	4	6
B472	0.080	0.004	3.214	0.142	1.378	0.168	1.266	0.192	0.514	0.143	2.26	0.15	0	3
B475	0.109	0.033	0.279	0.631	1.083	0.422	0.496	0.485	99.999	99.999	6.13	0.30	3	4
B480	0.035	0.033	1.123	0.631	1.697	0.422	1.982	0.485	99.999	99.999	5.36	0.30	2	4
B483	0.089	0.033	0.004	0.631	1.014	0.422	-1.270	0.485	99.999	99.999	5.75	0.30	3	4
B484	0.044	0.033	1.235	0.631	0.980	0.422	1.539	0.485	99.999	99.999	5.87	0.30	3	4
B486	0.029	0.038	-1.473	0.064	-0.057	0.057	99.999	99.999	99.999	99.999	3.22	0.06	1	5
G001	0.133	0.003	2.187	0.104	1.866	0.115	1.915	0.131	0.936	0.098	2.37	0.10	0	7

Table A.2. continued.

Cluster	Mg ₂ mag	eMg ₂ mag	Mgb Å	eMgb Å	Fe5270 Å	eFe5270 Å	Fe5335 Å	eFe5335 Å	Fe5406 Å	eFe5406 Å	H β Å	eH β Å	y ¹	Set ²
G002	0.053	0.016	-0.155	0.026	1.138	0.023	99.999	99.999	99.999	99.999	2.12	0.03	0	5
B189D	0.079	0.033	1.217	0.631	0.807	0.422	2.252	0.485	99.999	99.999	4.41	0.30	1	4
B020D	0.092	0.016	1.713	0.653	0.340	0.805	0.897	0.917	0.602	0.696	3.25	0.49	0	3
B103D	0.193	0.033	3.291	0.631	2.631	0.422	2.386	0.485	99.999	99.999	1.74	0.30	0	4
G327	0.053	0.033	0.934	0.631	0.876	0.422	0.320	0.485	99.999	99.999	3.00	0.30	0	4
VDB0	0.031	0.002	0.186	0.088	0.598	0.101	0.568	0.116	0.366	0.087	4.50	0.07	1	6
NB16	0.066	0.013	1.610	0.200	1.180	0.090	0.970	0.110	0.500	0.080	3.34	0.08	4	2
NB89	0.123	0.013	2.430	0.200	1.910	0.090	1.630	0.110	1.020	0.070	2.04	0.09	0	2
B012D	0.076	0.033	1.197	0.631	1.899	0.422	2.016	0.485	99.999	99.999	7.27	0.30	2	4
B025D [‡]	0.250	0.024	4.182	0.955	1.875	1.094	2.463	1.258	0.035	1.008	0.11	0.86	0	3
B026D [‡]	0.185	0.033	2.467	0.631	1.764	0.422	1.160	0.485	99.999	99.999	0.02	0.30	0	4
B041D	0.126	0.020	0.685	0.851	1.416	0.945	1.897	1.075	1.019	0.817	2.00	0.65	0	3
B043D [‡]	0.100	0.033	1.661	0.631	1.697	0.422	0.532	0.485	99.999	99.999	0.04	0.30	0	4
B046D [‡]	0.230	0.026	3.245	1.091	2.712	1.255	3.013	1.454	1.154	1.160	2.15	0.76	0	3
B090D	0.291	0.007	4.122	0.298	2.604	0.349	2.241	0.408	1.732	0.310	1.54	0.23	0	3
B091D	0.112	0.033	2.431	0.631	1.289	0.422	2.117	0.485	99.999	99.999	1.98	0.30	0	4
B111D	0.070	0.033	1.495	0.631	1.014	0.422	1.160	0.485	99.999	99.999	5.73	0.30	2	4
B215D [‡]	0.187	0.009	2.449	0.392	1.676	0.463	1.450	0.547	1.061	0.414	1.82	0.28	0	3
B240D	0.043	0.033	1.624	0.631	0.179	0.422	0.602	0.485	99.999	99.999	2.01	0.30	7	4
B248D [‡]	0.286	0.033	3.558	0.631	3.316	0.422	4.468	0.485	99.999	99.999	0.04	0.30	0	4
B257D	0.040	0.033	0.896	0.631	-1.365	0.422	0.036	0.485	99.999	99.999	5.66	0.30	2	4
B289D	0.143	0.033	2.624	0.631	2.565	0.422	-1.270	0.485	99.999	99.999	3.54	0.30	0	4
B292D	0.229	0.033	3.934	0.631	3.381	0.422	0.952	0.485	99.999	99.999	2.15	0.30	0	4
B344D	0.121	0.001	2.517	0.022	2.054	0.024	1.679	0.028	1.372	0.021	2.66	0.02	0	6
DAO25 [‡]	0.060	0.033	2.290	0.631	1.289	0.422	-1.122	0.485	99.999	99.999	1.79	0.30	0	4
DAO30	0.151	0.033	2.273	0.631	3.734	0.422	3.148	0.485	99.999	99.999	3.59	0.30	7	4
DAO47	0.044	0.033	1.179	0.631	-0.033	0.422	3.115	0.485	99.999	99.999	4.20	0.30	2	4
V031	0.052	0.033	1.366	0.631	0.319	0.422	0.812	0.485	99.999	99.999	6.01	0.30	2	4
BA11	0.120	0.033	3.054	0.631	1.697	0.422	0.672	0.485	99.999	99.999	1.07	0.30	0	4
B514	0.062	0.003	0.300	0.137	0.176	0.154	1.279	0.169	0.282	0.159	2.32	0.13	0	7
MCGC1	0.041	0.007	0.566	0.290	0.489	0.327	0.005	0.379	0.397	0.276	1.84	0.29	0	7
MCGC8	0.093	0.003	1.334	0.115	1.400	0.128	1.206	0.147	1.041	0.109	1.98	0.10	0	6
MCGC10	0.031	0.003	0.395	0.104	0.633	0.118	0.427	0.136	0.677	0.100	2.93	0.09	0	6

¹ y=BLCC (young cluster) from Fusi Pecci et al. (2005) 0– old cluster; 1– color selected; 2– H_{β} selected; 3– color and H_{β} selected; 4– reportedly young objects by other authors and candidates BLCC (table 2)

7– classified young by Caldwell et al. (2009)

² Dataset label: 0– Trager et al. (1998), 1– Puzia et al. (2005), 2– Beasley et al. (2004), 3– WHT data, 4– Perrett et al. (2002), 5– Huchra et al. (1991), 6– TNG data, 7– LOI data

[‡] B025D, B026D, B043D, B046D, B215D, B248D and DAO25 are classified by Caldwell et al. (2009) to be not-clusters and in the following analysis are not considered.

Table A.3. Metallicities for M31 globular clusters.

Cluster	[Fe/H] dex	e[Fe/H] dex	Cluster	[Fe/H] dex	e[Fe/H] dex	Cluster	[Fe/H] dex	e[Fe/H] dex	Cluster	[Fe/H] dex	e[Fe/H] dex
B001	-0.42	0.32	B085	-2.10	0.26	B183	-0.47	0.15	B344	-0.80	0.21
B003	-0.99	0.48	B086	-1.80	0.18	B184	-0.01	0.22	B347	-1.91	0.24
B004	-1.00	0.41	B088	-1.94	0.52	B185	-0.50	0.20	B348	-0.75	0.23
B005	-0.82	0.38	B090	-0.17	0.26	B187	-1.52	0.54	B350	-1.54	0.31
B006	-0.59	0.41	B092	-1.14	0.23	B188	-1.51	0.51	B352	-0.96	0.24
B008	-0.47	0.35	B093	-0.74	0.38	B190	-0.80	0.39	B356	-1.62	0.32
B009	-1.55	0.23	B094	-0.35	0.30	B193	0.04	0.15	B357	-0.88	0.20
B010	-1.64	0.68	B095	-0.79	0.66	B197	0.02	0.21	B358	-1.85	0.19
B011	-1.71	0.24	B096	-0.23	0.19	B198	-0.55	0.34	B365	-1.32	0.20
B012	-1.91	0.21	B097	-0.95	0.42	B199	-1.70	0.51	B366	-2.14	0.39
B013	-0.74	0.51	B098	-0.45	0.19	B200	-0.43	0.32	B370	-1.98	0.50
B015	0.37	0.15	B099	-0.86	0.36	B201	-1.08	0.16	B372	-1.07	0.53
B016	-0.53	0.34	B103	-0.43	0.15	B203	-0.64	0.36	B373	-0.59	0.47
B017	-0.82	0.24	B105	-0.93	0.42	B204	-0.39	0.15	B375	-0.87	0.22
B018	-0.77	0.39	B106	-0.81	0.28	B205	-1.16	0.15	B377	-1.55	0.33
B019	-0.74	0.15	B107	-1.20	0.15	B206	-1.16	0.15	B378	-1.38	0.51
B020	-0.83	0.15	B110	-0.64	0.28	B207	-1.10	0.44	B379	-0.53	0.15
B021	-0.74	0.37	B111	-0.85	0.71	B208	-0.32	0.30	B381	-1.10	0.22
B022	-1.30	0.59	B112	0.13	0.15	B209	-0.98	0.41	B382	-1.16	0.44
B023	-0.91	0.15	B115	0.06	0.15	B211	-1.92	0.29	B383	-0.47	0.15
B024	-0.59	0.15	B116	-0.50	0.34	B212	-2.07	0.28	B384	-0.59	0.15
B025	-1.53	0.79	B117	-1.78	0.23	B213	-0.69	0.36	B386	-1.09	0.15
B026	-0.09	0.25	B119	-0.25	0.28	B214	-1.00	0.47	B387	-1.37	0.21
B027	-1.64	0.16	B122	-1.20	0.44	B215	-0.33	0.19	B391	-0.96	0.48
B029	0.02	0.21	B125	-1.99	0.34	B217	-0.84	0.39	B393	-1.03	0.24
B030	-0.14	0.26	B126	-1.48	0.19	B218	-0.71	0.18	B397	-0.90	0.22
B031	-1.73	0.39	B127	-0.54	0.15	B219	-0.55	0.26	B398	-0.41	0.18
B032	0.03	0.29	B129	-0.69	0.36	B220	-1.09	0.42	B399	-1.63	0.18
B033	-1.12	0.47	B130	-1.19	0.44	B221	-0.83	0.39	B400	-1.23	0.47
B034	-0.96	0.38	B131	-0.15	0.15	B224	-1.68	0.28	B401	-1.98	0.26
B035	-0.67	0.38	B134	-0.79	0.15	B225	-0.35	0.15	B403	-0.27	0.35
B037	-0.60	0.37	B135	-1.46	0.48	B228	-0.86	0.24	B405	-1.28	0.15
B038	-1.86	0.52	B137	-1.26	0.54	B230	-2.36	0.24	B407	-0.65	0.15
B039	-0.62	0.24	B140	-0.29	0.29	B231	-0.85	0.39	B431*	-1.49	0.33
B041	-1.14	0.47	B141	-1.71	0.58	B232	-2.01	0.23	B457	0.17	0.15
B042	-0.86	0.27	B143	-0.09	0.15	B233	-1.54	0.17	B467	-2.29	0.25
B044	-1.09	0.30	B144	-0.55	0.30	B234	-0.72	0.15	B468	-0.88	0.25
B045	-1.01	0.50	B146	-0.53	0.31	B235	-0.73	0.17	B472	-0.71	0.15
B046	-0.99	0.36	B147	0.02	0.15	B238	-0.43	0.17	B486	-1.91	0.46
B047	-0.28	0.22	B148	-0.70	0.27	B239	-1.46	0.28	B514	-2.06	0.16
B048	-0.55	0.55	B149	-1.00	0.45	B240	-1.74	0.19	G001	-0.73	0.15
B050	-1.21	0.45	B151	-0.44	0.16	B272	-0.81	0.38	G002	-1.63	0.18
B051	-0.73	0.51	B152	-1.53	0.29	B283	-0.52	0.34	G327	-1.79	0.52
B054	-0.10	0.24	B153	-0.13	0.25	B292	-1.54	0.37	NB16	-1.27	0.15
B055	-0.31	0.29	B154	0.03	0.15	B293	-1.59	0.23	NB89	-0.70	0.15
B056	0.07	0.20	B155	-0.08	0.19	B298	-1.78	0.22	B020D	-1.52	0.59
B058	-1.02	0.21	B156	-1.30	0.34	B301	-1.13	0.32	B041D	-1.49	0.74
B059	-0.75	0.40	B158	-0.74	0.15	B304	-1.38	0.33	B090D	-0.09	0.16
B060	-1.13	0.55	B159	-0.77	0.38	B305	-1.04	0.42	B091D	-0.73	0.37
B061	-0.52	0.33	B161	-0.74	0.37	B306	-1.10	0.43	B103D	-0.22	0.27
B063	-0.76	0.17	B162	0.02	0.31	B310	-1.57	0.34	B240D*	-1.74	0.53
B064	-1.37	0.21	B163	-0.08	0.15	B311	-1.71	0.53	B289D	-1.28	0.54
B065	-1.24	0.45	B164	-0.41	0.31	B312	-1.18	0.37	B292D	-0.20	0.27
B068	-0.41	0.17	B165	-1.66	0.29	B313	-0.86	0.19	B344D	-0.64	0.15
B070	-1.42	0.43	B167	-0.25	0.28	B316	-0.79	0.38	DAO30*	-0.26	0.30
B071	0.05	0.24	B169	0.07	0.23	B317	-1.92	0.36	BA11	-0.82	0.40
B072	-0.28	0.29	B171	-0.17	0.15	B328	-2.17	0.30	MCGC1	-2.16	0.28
B073	-0.11	0.25	B174	-1.05	0.22	B335	-0.89	0.40	MCGC8	-1.27	0.15
B075	-1.33	0.46	B178	-1.16	0.21	B337	-1.08	0.15	MCGC10	-2.07	0.15
B076	-0.89	0.40	B179	-0.98	0.27	B338	-1.23	0.22			
B082	-0.55	0.33	B180	-0.75	0.18	B341	-0.96	0.40			
B083	-1.73	0.46	B182	-0.97	0.35	B343	-1.28	0.15			

Appendix B: Spearman correlation matrix for Lick indices and metallicity

During the first phases of the present study we considered the largest set of Lick indices to search for the best candidates to be used as metallicity indicators for our scale. As a useful tool for this choice we computed the matrix of Spearman rank correlation coefficients (Press et al. (1992)) for a set of indices in the T98 system and metallicity for Galactic GCs. Since this matrix can be of general interest, we present it here as Table B.1 below. It must be recalled that these correlations coefficients are computed using a sample of nearly-uniformly *old stellar populations*, hence it refers only to classical old globulars.

Table B.1. Spearman rank correlation coefficients.

	[Fe/H] _{ZW}	CN1	CN2	Ca4227	G4300	Ca4455	Fe4531	C24668	H β	Fe5015	Mg1	Mg2	Mgb	Fe5270	Fe5335	Fe5709	NaD	TiO1	MgFe
[Fe/H] _{ZW}	1.000	0.711	0.620	0.598	0.885	0.684	0.843	0.331	-0.875	0.902	0.912	0.958	0.858	0.860	0.703	0.669	0.772	0.613	0.922
CN1	0.711	1.000	0.961	0.760	0.784	0.537	0.375	0.632	-0.676	0.777	0.703	0.672	0.529	0.527	0.765	0.505	0.627	0.618	0.652
CN2	0.620	0.961	1.000	0.718	0.699	0.566	0.233	0.647	-0.554	0.694	0.618	0.556	0.426	0.424	0.681	0.392	0.537	0.613	0.532
Ca4227	0.598	0.760	0.718	1.000	0.630	0.387	0.301	0.311	-0.542	0.689	0.630	0.600	0.505	0.583	0.632	0.439	0.583	0.637	0.620
G4300	0.885	0.784	0.699	0.630	1.000	0.605	0.664	0.390	-0.868	0.877	0.873	0.855	0.787	0.696	0.659	0.654	0.662	0.576	0.806
Ca4455	0.684	0.537	0.566	0.387	0.605	1.000	0.569	0.238	-0.419	0.755	0.676	0.652	0.667	0.615	0.559	0.279	0.461	0.422	0.630
Fe4531	0.843	0.375	0.233	0.301	0.664	0.569	1.000	0.029	-0.679	0.679	0.706	0.863	0.873	0.814	0.493	0.615	0.598	0.230	0.887
C24668	0.331	0.632	0.647	0.311	0.390	0.238	0.029	1.000	-0.328	0.265	0.365	0.279	0.083	0.056	0.431	0.191	0.191	0.453	0.147
H β	-0.875	-0.676	-0.554	-0.542	-0.868	-0.419	-0.679	-0.328	1.000	-0.792	-0.831	-0.873	-0.728	-0.699	-0.659	-0.809	-0.811	-0.495	-0.792
Fe5015	0.902	0.777	0.694	0.689	0.877	0.755	0.679	0.265	-0.792	1.000	0.853	0.887	0.838	0.799	0.775	0.507	0.735	0.657	0.885
Mg1	0.912	0.703	0.618	0.630	0.873	0.676	0.706	0.365	-0.831	0.853	1.000	0.885	0.745	0.721	0.713	0.681	0.752	0.505	0.787
Mg2	0.958	0.672	0.556	0.600	0.855	0.652	0.863	0.279	-0.873	0.887	0.885	1.000	0.922	0.848	0.672	0.647	0.792	0.510	0.946
Mgb	0.858	0.529	0.426	0.505	0.787	0.667	0.873	0.083	-0.728	0.838	0.745	0.922	1.000	0.814	0.596	0.569	0.689	0.444	0.951
Fe5270	0.860	0.527	0.424	0.583	0.696	0.615	0.814	0.056	-0.699	0.799	0.721	0.848	0.814	1.000	0.502	0.502	0.806	0.569	0.892
Fe5335	0.703	0.765	0.681	0.632	0.659	0.559	0.493	0.431	-0.659	0.775	0.713	0.672	0.596	0.502	1.000	0.608	0.593	0.537	0.708
Fe5709	0.669	0.505	0.392	0.439	0.654	0.279	0.615	0.191	-0.809	0.507	0.681	0.647	0.569	0.502	0.608	1.000	0.689	0.208	0.623
NaD	0.772	0.627	0.537	0.583	0.662	0.461	0.598	0.191	-0.811	0.735	0.752	0.792	0.689	0.806	0.593	0.689	1.000	0.480	0.762
TiO1	0.613	0.618	0.613	0.637	0.576	0.422	0.230	0.453	-0.495	0.657	0.505	0.510	0.444	0.569	0.537	0.208	0.480	1.000	0.527
MgFe	0.922	0.652	0.532	0.620	0.806	0.630	0.887	0.147	-0.792	0.885	0.787	0.946	0.951	0.892	0.708	0.623	0.762	0.527	1.000